J Neurophysiol 89: 2707–2725, 2003.
First published January 15, 2003; 10.1152/jn.00845.2002.

Cellular and Network Mechanisms of Slow Oscillatory Activity (<1 Hz) and Wave Propagations in a Cortical Network Model

Albert Compte,[1,2] Maria V. Sanchez-Vives,[2] David A. McCormick,[3] and Xiao-Jing Wang[1]

[1]*Volen Center for Complex Systems, Brandeis University, Waltham, Massachusetts 02454;* [2]*Instituto de Neurociencias, Universidad Miguel Hernández-Consejo Superior Investigaciones Científicas, 03550 San Juan de Alicante, Spain; and* [3]*Section of Neurobiology, Yale University School of Medicine, New Haven, Connecticut 96510*

Submitted 24 September 2002; accepted in final form 20 December 2002

Compte, Albert, Maria V. Sanchez-Vives, David A. McCormick, and Xiao-Jing Wang. Cellular and network mechanisms of slow oscillatory activity (<1 Hz) and wave propagations in a cortical network model. *J Neurophysiol* 89: 2707–2725, 2003. First published January 15, 2003; 10.1152/jn.00845.2002. Slow oscillatory activity (<1 Hz) is observed in vivo in the cortex during slow-wave sleep or under anesthesia and in vitro when the bath solution is chosen to more closely mimic cerebrospinal fluid. Here we present a biophysical network model for the slow oscillations observed in vitro that reproduces the single neuron behaviors and collective network firing patterns in control as well as under pharmacological manipulations. The membrane potential of a neuron oscillates slowly (at <1 Hz) between a down state and an up state; the up state is maintained by strong recurrent excitation balanced by inhibition, and the transition to the down state is due to a slow adaptation current (Na^+-dependent K^+ current). Consistent with in vivo data, the input resistance of a model neuron, on average, is the largest at the end of the down state and the smallest during the initial phase of the up state. An activity wave is initiated by spontaneous spike discharges in a minority of neurons, and propagates across the network at a speed of 3–8 mm/s in control and 20–50 mm/s with inhibition block. Our work suggests that long-range excitatory patchy connections contribute significantly to this wave propagation. Finally, we show with this model that various known physiological effects of neuromodulation can switch the network to tonic firing, thus simulating a transition to the waking state.

Cortical oscillatory activity as measured by electroencephalogram (EEG) is a clear signature of the general state of the brain. The waking state and the rapid-eye-movement (REM) phase of sleep are characterized by low-amplitude fast oscillations (Gray et al. 1989; Steriade et al. 1996) of a generally low spatiotemporal coherence (Destexhe et al. 1999). In contrast, during slow-wave sleep and anesthesia, the brain shows pronounced oscillatory activity at a variety of frequencies often with remarkable long range synchrony (Bullock and McClune 1989; Destexhe et al. 1999; Steriade et al. 1993a, 1996). During slow-wave sleep, low-frequency (<1 Hz) oscillations are visible both in the EEG, and in extracellular and intracellular recordings (Achermann and Borbély 1997; Lampl et al. 1999; Steriade et al. 1993b,c, 1996; Stern et al. 1997). Lesion studies have shown that this type of rhythmic activity originates in the cortex and is then reflected in subcortical structures (Amzica and Steriade 1995; Steriade et al. 1993c). Intracellular recordings in vivo showed that the slow oscillation is mediated by two phases: a period in which nearly all cell types within the cerebral cortex are depolarized and generate action potentials at a low rate (the so-called up state) interdigitated with a period of hyperpolarization and relative inactivity (the down state). The transition from the up to down states has been proposed to occur either in response to synaptic "fatigue" or depression (Contreras et al. 1996) or to the build-up of activity-dependent K^+ conductances (Sanchez-Vives and McCormick 2000). A gradual increase in input resistance of pyramidal cells during the up state in vivo has been taken to indicate a steady decrease of a specific ionic conductance, suggesting a stronger role of depression of excitatory synapses over the activation of K^+ conductances in the transition from the up to the down state (Contreras et al. 1996; Timofeev et al. 2000b).

Recently, spontaneous activity similar to the slow oscillations (<1 Hz) recorded in vivo has been described in an in vitro slice preparation of cerebral cortex when maintained in an ionically modified artificial cerebral spinal fluid (ACSF) solution that mimics ionic concentrations in situ more closely than the solutions traditionally used for cortical slice preparations (Sanchez-Vives and McCormick 2000). This helped to identify candidate cellular and circuit mechanisms underlying the generation of slow oscillations and wave propagation in ferret visual cortex slices. For example, pharmacological manipulations show that this activity depends on excitatory transmission through AMPA and *N*-methyl-D-aspartate (NMDA) receptors, suggesting a critical role of recurrent excitatory connections. Open issues remain in relation to the two main aspects of slowly oscillating cortical activity: the membrane potential sudden transition between and up state and a down state and the propagation of activity across the cortical network. Evidence suggests that the transition from the up state to down state is induced by the opening of a K^+ conductance (Sanchez-Vives and McCormick 2000), whose time course has led to the hypothesis that it is a slow Na^+-dependent K^+ conductance g_{KNa} known to exist in these neurons (Sanchez-Vives et al. 2000). This raises the question of how an increase of g_{KNa} in a pyramidal cell could be compatible with an increase of its input resistance observed during the course of an up state. Another intriguing aspect of these membrane fluctuations is the sharpness of the transitions between the up and the down states, where the relative contribution of intrinsic and network mecha-

Address for reprint requests: A. Compte, Instituto de Neurosciencias, Universidad Miguel Hernández-CSIC, 03550 San Juan de Alicante, Spain (E-mail: acompte@umh.es).

nisms remains to be established. On the other hand, as observed experimentally, an up state episode consists of barrages of synaptic activity that initiate earlier in infragranular laminae and occur in all cortical layers. This reverberatory network activity propagates across the slice at ~10 mm/s and is followed by a silent period of 2–4 s. Blocking $GABA_A$-mediated inhibition results in epileptiform discharges that propagate along the slice at ~100 mm/s. The ability of a cortical network to sustain two propagation velocities has been studied mathematically by Golomb and Ermentrout (2001) for a simple model where each cell is an integrate-and-fire neuron and is allowed to fire only one spike. It remains to be examined how these two wave propagation modes can be realized in a biophysically realistic network model of conductance-based neurons.

The combined results obtained from the in vivo and in vitro preparations provide a framework to build a physiologically realistic network model of the slow oscillation in a cortical slice. We present here this biologically realistic network model, and we use it to address the aforementioned questions about the rhythmogenesis and wave propagation. We then speculate about how our model could relate to slow oscillations during natural slow-wave sleep and activity in the waking state in vivo.

METHODS

The network model consists of a population of 1,024 pyramidal cells and 256 interneurons equidistantly distributed on a line and interconnected through biologically plausible synaptic dynamics. Some of the intrinsic parameters of the cells are randomly distributed, so that the populations are heterogeneous. This and the random connectivity (determined by the synaptic probability distributions; see Fig. 2*A*) are the only sources of noise in the network.

Model neurons

Especially in vivo, intracellular voltage records show clear transitions between two well-defined stable membrane potentials (Cowan and Wilson 1994; Stern et al. 1997). It has been argued that intrinsic channels may shape the neuronal membrane potential via an inward rectifier K^+ channel (I_{AR}) and a slowly inactivating K^+ channel activated by depolarization (I_{KS}) (Nisenbaum et al. 1994; Wilson 1992; Wilson and Kawaguchi 1996). In our model pyramidal neurons, we include these and other channels found in cortical pyramidal cells.

Our model pyramidal cells have a somatic and a dendritic compartment (Pinsky and Rinzel 1994). The spiking currents, I_{Na} and I_K, are located in the soma, together with a leak current I_L, a fast A-type K^+ current I_A, a non-inactivating slow K^+ current I_{KS}, and a Na^+-dependent K^+ current I_{KNa}. The dendrite contains a high-threshold Ca^{2+} current I_{Ca}, a Ca^{2+}-dependent K^+-current I_{KCa}, a non-inactivating (*persistent*) Na^+ current I_{NaP}, and an inward rectifier (activated by hyperpolarization) non-inactivating K^+ current I_{AR}. The dynamical equations for the somatic voltage (V_s) and the dendritic voltage (V_d) are

$$C_m A_s \frac{dV_s}{dt} = -A_s(I_L + I_{Na} + I_K + I_A + I_{KS} + I_{KNa}) - I_{syn,s} - g_{sd}(V_s - V_d)$$

$$C_m A_d \frac{dV_d}{dt} = -A_d(I_{Ca} + I_{KCa} + I_{NaP} + I_{AR}) - I_{syn,d} - g_{sd}(V_d - V_s)$$

with the membrane capacitance $C_m = 1\ \mu F/cm^2$ and the areas being $A_s = 0.015\ mm^2$ and $A_d = 0.035\ mm^2$ for the soma and dendrite, respectively. The coupling between soma and dendrite is determined by $g_{sd} = 1.75 \pm 0.1\ \mu S$ (axial resistance 0.57 MΩ, standard deviation indicates the degree to which this parameter is randomly varied from cell to cell). $I_{syn,s}$ and $I_{syn,d}$ are the synaptic currents impinging on the soma and dendrites, respectively. In our simulations, all excitatory synapses target the dendritic compartment and all inhibitory synapses are localized on the somatic compartment of postsynaptic pyramidal neurons.

Interneurons are modeled with just Hodgkin-Huxley spiking currents, I_{Na} and I_K, and a leak current I_L in their single compartment

$$C_m A_i \frac{dV}{dt} = -A_i(I_L + I_{Na} + I_K) - I_{syn,i}$$

with the total neuronal surface area being $A_i = 0.02\ mm^2$.

Ion channel kinetics and conductances

All ion channels are modeled following the Hodgkin-Huxley formalism, with gating variables x governed by the first-order kinetics equation $dx/dt = \phi\,[\alpha_x(V)(1 - x) - \beta_x(V)x] = \phi[x_\infty(V) - x]/\tau_x(V)$. ϕ being the temperature factor ($\phi = 1$ unless otherwise indicated).

For pyramidal cells, the sodium and potassium spiking currents are modeled following (Wang 1998) with slight variations. The sodium current $I_{Na} = g_{Na} m_\infty^3 h(V - V_{Na})$ has a maximum conductance of $g_{Na} = 50\ mS/cm^2$, its rapid activation variable is replaced by its steady-state $m_\infty = \alpha_m/(\alpha_m + \beta_m)$ with $\alpha_m = 0.1(V + 33)/[1 - \exp(-(V + 33)/10)]$ and $\beta_m = 4\exp(-(V + 53.7)/12)$ and the inactivation variable has $\alpha_h = 0.07\exp(-(V + 50)/10)$ and $\beta_h = 1/[1 + \exp(-(V + 20)/10)]$. The temperature factor is $\phi = 4$. The delayed rectifier $I_K = g_K n^4(V - V_K)$ has a maximal conductance $g_K = 10.5\ mS/cm^2$ and its inactivation kinetics are set by $\alpha_n = 0.01(V + 34)/[1 - \exp(-(V + 34)/10)]$ and $\beta_n = 0.125\exp[-(V + 44)/25]$, with $\phi = 4$. The leakage current $I_L = g_L(V - V_L)$ is a passive channel with conductance $g_L = 0.0667 \pm 0.0067\ mS/cm^2$ (Gaussian-distributed in the population, mean ± SD given). The fast A-type K^+-channel is as in Golomb and Amitai (1997); $I_A = g_A m_\infty^3 h(V - V_K)$ has its fast activation variable replaced by its steady-state $m_\infty = 1/[1 + \exp(-(V + 50)/20)]$ and the inactivation variable is governed by $h_\infty = 1/[1 + \exp((V + 80)/6)]$ and $\tau_h = 15$ ms. Its maximal conductance is $g_A = 1\ mS/cm^2$. The non-inactivating K^+-channel is modeled as in (Wang 1999a) but with no inactivation variable: $I_{KS} = g_{KS} m(V - V_K)$. It has a maximal conductance $g_{KS} = 0.576\ mS/cm^2$ and an activation controlled by $m_\infty = 1/[1 + \exp(-(V + 34)/6.5)]$ and $\tau_m = 8/[\exp(-(V + 55)/30) + \exp((V + 55)/30)]$. The remaining currents are modeled with instantaneous activation because their activation is sufficiently fast and removing these additional variables significantly reduces the time required to perform our network simulations.

The persistent sodium channel $I_{NaP} = g_{NaP} m_\infty^3(V - V_{Na})$ has maximal conductance $g_{NaP} = 0.0686\ mS/cm^2$, it activates instantaneously according to $m_\infty = 1/[1 + \exp(-(V + 55.7)/7.7)]$ and it does not inactivate. It is borrowed with parameter modification from (Fleidervish et al. 1996). The inwardly rectifying K^+ channel was modeled as in (Stern et al. 1997; Spain et al. 1987) and adjusting the parameters: $I_{AR} = g_{AR} h_\infty(V - V_K)$ activates instantaneously below a low-lying threshold following $h_\infty = 1/[1 + \exp((V + 75)/4)]$ and it has a maximal conductance $g_{AR} = 0.0257\ mS/cm^2$. The high-threshold Ca^{2+}-channel $I_{Ca} = g_{Ca} m_\infty^2(V - V_{Ca})$ has $g_{Ca} = 0.43\ mS/cm^2$ and is instantaneously activated at very depolarized voltages, thus making it effectively a very transient current. The voltage dependency is given by $m_\infty = 1/[1 + \exp(-(V + 20)/9)]$. The concentration of intracellular calcium, $[Ca^{2+}]$, follows first-order kinetics as $d[Ca^{2+}]/dt = -\alpha_{Ca} A_d I_{Ca} - [Ca^{2+}]/\tau_{Ca}$ with $\alpha_{Ca} = 0.005\ \mu M/(nA \cdot ms)$ and $\tau_{Ca} = 150$ ms. The Ca^{2+}-dependent K^+ channel $I_{KCa} = g_{KCa}[Ca^{2+}]/([Ca^{2+}] + K_D)(V - V_K)$ (with $K_D = 30\ \mu M$) activates instantaneously in the presence of intracellular calcium $[Ca^{2+}]$, and it has a maximal conductance $g_{KCa} = 0.57\ mS/cm^2$. All the mechanisms involving intracellular calcium are taken from Wang (1998). As for the intracellular sodium concentration $[Na^+]$, its dynamics are somewhat more involved because they incorporate a Na-K pump (Li et al. 1996): $d[Na^+]/dt = -\alpha_{Na}(A_s I_{Na} + A_d I_{NaP}) - R_{pump}\{[Na^+]^3/([Na^+]^3 +$

$15^3) - [Na^+]_{eq}^3/([Na^+]_{eq}^3 + 15^3)\}$, with $\alpha_{Na} = 0.01$ mM/(nA · ms), $R_{pump} = 0.018$ mM/ms, and $[Na^+]_{eq} = 9.5$ mM. The Na^{2+}-dependent K^+ channel $I_{KNa} = g_{KNa} w_\infty([Na^+])(V - V_K)$ has a conductance $g_{KNa} = 1.33$ mS/cm^2 and $w_\infty([Na^+]) = 0.37/[1 + (38.7/[Na^+])^{3.5}]$ (Bischoff et al. 1998). The kinetics for $[Na^+]$ and I_{KNa} are taken from (Liu 1999; Wang et al. 2002). For all these channels, the reversal potentials used are $V_L = -60.95 \pm 0.3$ mV, $V_{Na} = 55$ mV, $V_K = -100$ mV, and $V_{Ca} = 120$ mV.

For the last three figures, a slight modification in the implementation of the I_{KNa} current was introduced because we realized that I_{KNa} was continuously contributing a sizable $[Na^+]$-independent, voltage-independent hyperpolarizing current that was confounded with the leakage current. Because for those figures we were interested in changing independently g_{KNa} and g_L, we opted to subtract the constant part from I_{KNa}: $I_{KNa} = g_{KNa}(w_\infty([Na^+]) - w_\infty([Na^+]_{eq}))(V - V_K)$ and change the leakage properties to compensate for this: $g_L = 0.07$ mS/cm^2 and $V_L = -62.8$ mV.

For interneurons, the model was taken from Wang and Buzsáki (1996). The sodium current $I_{Na} = g_{Na} m_\infty^3 h(V - V_{Na})$ has a maximal conductance $g_{Na} = 35$ mS/cm^2, and its rapid activation is replaced by its steady-state value $m_\infty = \alpha_m/(\alpha_m + \beta_m)$ with $\alpha_m = 0.5(V + 35)/[1 - \exp(-(V + 35)/10)]$ and $\beta_m = 20\exp(-(V + 60)/18)$. The inactivation gating variable is controlled by $\alpha_h = 0.35\exp(-(V + 58)/20)$ and $\beta_h = 5/[1 + \exp(-(V + 28)/10)]$. The delayed rectifier $I_K = g_K n^4(V - V_K)$ has $g_K = 9$ mS/cm^2 and it activates with kinetics given by $\alpha_n = 0.05(V + 34)/[1 - \exp(-(V + 34)/10)]$ and $\beta_n = 0.625\exp(-(V + 44)/80)$. The leakage current $I_L = g_L(V - V_L)$ is a passive channel with conductance $g_L = 0.1025 \pm 0.0025$ mS/cm^2. The reversal potentials are $V_L = -63.8 \pm 0.15$ mV, $V_{Na} = 55$ mV, and $V_K = -90$ mV.

Model pyramidal neurons set according to these parameters fire at an average of 22 Hz when they are injected a depolarizing current of 0.25 nA for 0.5 s. The firing pattern corresponds to a regular spiking neuron with some adaptation, no bursting pattern was ever observed. In contrast, a model interneuron fires at ~75 Hz when equally stimulated and has the firing pattern of a fast spiking neuron.

Model synapses

Kinetics of synaptic currents is modeled as in (Wang 1999b): a postsynaptic current $I_{syn} = g_{syn} s(V - V_{syn})$ enters the postsynaptic neuron when the presynaptic neuron's action potential activates the gating variable $s(t)$ following $ds/dt = \alpha f(V_{pre}) - s/\tau$, with $f(V_{pre}) = 1/[1 + \exp(-(V_{pre} - 20)/2)]$. For AMPAR-mediated synaptic transmission, $\alpha = 3.48$, $\tau = 2$ ms, and $V_{syn} = 0$; while for inhibitory synaptic transmission $\alpha = 1$, $\tau = 10$ ms, and $V_{syn} = -70$ mV. In the case of NMDAR-mediated synaptic transmission, the gating variable follows a second-order kinetic scheme: $ds/dt = \alpha(1 - s) - s/\tau$, $dx/dt = \alpha_x f(V_{pre}) - x/\tau_x$ ($\alpha = 0.5$, $\tau = 100$ ms, $\alpha_x = 3.48$, $\tau_x = 2$ ms, $V_{syn} = 0$) so that the ensuing excitatory postsynaptic current (EPSC) has a slower rise phase and saturates at high presynaptic firing rates.

Unless specified otherwise, the synaptic conductances' maximal strengths are set to the following values: pyramidal to pyramidal: $g_{EE}^{AMPA} = 5.4$ nS, $g_{EE}^{NMDA} = 0.9$ nS; pyramidal to interneuron: $g_{EI}^{AMPA} = 2.25$ nS, $g_{EI}^{NMDA} = 0.5$ nS; interneuron to pyramidal: $g_{IE} = 4.15$ nS; and interneuron to interneuron: $g_{II} = 0.165$ nS. In Fig. 11 (except for *A, left*) the synaptic conductances are changed to $g_{EE}^{AMPA} = 5.75$ nS, $g_{EE}^{NMDA} = 0.75$ nS, $g_{EI}^{AMPA} = 2.75$ nS, $g_{EI}^{NMDA} = 0.6$ nS, $g_{IE} = 4.25$ nS, $g_{II} = 0.135$ nS. These values were chosen so that the network would show stable periodic propagating discharges with characteristics compatible with experimental observations. The precise network activity pattern is sensitive to these parameters but the qualitative presence of traveling waves and oscillations is robust to synaptic parameter changes (see examples in Fig. 6).

Cortical microcircuit connectivity

The neurons in the network are sparsely connected to each other through a fixed number of connections that are set at the beginning of the simulation. Neurons make 20 ± 5 (SD) contacts to their postsynaptic partners (multiple contacts onto the same target, but no autapses, are allowed). For each pair of neurons separated by a distance x in the network (see Fig. 2*A*), the probability that they are connected in each direction is decided by a Gaussian probability distribution centered at 0 and with a prescribed standard deviation σ: $P(x) = \exp(-x^2/2\sigma^2)/\sqrt{2\pi\sigma^2}$. In our simulations, the total length of the model network is assumed to be 5 mm, and we let $\sigma = 250$ μm for excitatory connections so that the typical size of a patch of connections coming from a single pyramidal neuron is 500 μm. This number is consistent with anatomical (Rockland 1985) data for local connections within ferret visual cortex. Anatomical studies have also shown that excitatory horizontal connections in cortex extend further away creating a periodic patchy pattern (Gilbert and Wiesel 1983; Rockland 1985). In some simulations, we include this by using a probability of connection given by $P(x) = [\exp(-x^2/2\sigma^2) + s\exp(-(x - d)^2/2\sigma^2) + s\exp(-(x + d)^2/2\sigma^2)]/(1 + 2s)/\sqrt{2\pi\sigma^2}$ so that additional probability of connection (whose strength is controlled by the parameter s) is added at a distance d of the soma (see Fig. 11*A, top right*). For inhibitory connections, a Gaussian probability distribution is also used but with a smaller standard deviation $\sigma = 125$ μm, except for simulations in Fig. 12, where $\sigma = 500$ μm is used. Anatomical and physiological data indicate that axonal arbors from inhibitory (basket) cells vary considerably, ranging from narrow to widespread (Crook et al. 1998). Here we mostly work with the narrow inhibition architecture but we also briefly explore the case of broader inhibition (Fig. 12).

Robustness of the model

The model network that we present here has proven its robustness to parameter modification in a variety of tests. The model is robust to connectivity sparsity and randomness and to neuronal inhomogeneity. Furthermore, a certain amount of randomness and heterogeneity seems to confer more stability to smooth wave propagation. Also, intrinsic neuronal properties can be varied substantially without changing the essential propagation and oscillation properties. Using a network of integrate-and-fire neurons, instead of Hodgkin-Huxley neurons, shows similar network dynamics (see van Vreeswijk and Hansel 2001; Wang 1999b for non-traveling slow oscillations), but the model cannot reproduce experimental intracellular data quantitatively. However, as indicated by Goldman et al. (2001) in a different context, there are some intrinsic parameters that do affect the collective network dynamics importantly. The reversal leak potential, for instance, controls very finely the excitability of the neurons, and its mean value across the population has very marked effects on the frequency of the slow oscillations. However, the standard deviation with which the reversal leak potential is distributed across the neuronal population does not have such an important effect on the activity characteristics. In particular, increasing threefold the reversal leak potential standard deviation augments the slow oscillation frequency by just 50% (from 0.27 to 0.4 Hz), the wave velocity 40% (from 5 to 7 mm/s), and the overall firing frequency 60% (from 1.1 to 1.8 Hz). Instead, with the same manipulation in a network with blocked excitatory synaptic transmission, the average spontaneous rate of firing of the network increases more than fourfold (from 0.06 to 0.26 Hz) and the number of spontaneously active neurons more than doubles (from 12 to 30%). This implies that the model is robust with respect to the exact fraction of neurons spontaneously active in the absence of synaptic excitation, but it is more sensitive to the overall excitability level of the network. As for neuron number, our simulations show that doubling or halving the number of neurons in our model network does not change either the oscillation frequency, or the wave propagation velocity, or the

average firing rate. This is so because the connectivity of the model is unaffected by the number of neurons. Any given neuron connects to an average of 20 postsynaptic cells independently of the size of the network.

Numerical methods

The model was implemented in a C++ code and simulated using a forth-order Runge-Kutta method with a time step of 0.06 ms.

Experimental methods

Experimental data depicted in Fig. 1 was collected extracellularly in prefrontal cortex slices of the ferret. Details of the methods can be found in Sanchez-Vives and McCormick, 2000.

RESULTS

Excitatory synaptic block reveals spontaneous neuronal firing

Extracellular multiple unit recordings in layer V revealed the basic characteristics of the slow oscillation in vitro, including the recurrence of synchronized bursts of activity in neighboring neurons, and the presence of spontaneous activity between up states (Fig. 1, *B–D*). The rate of firing of this multiple unit activity typically decreased following an up state but increased prior to the onset of the next up state (Fig. 1, *B–D*). At least some of this spontaneous activity was not dependent upon fast glutamatergic excitation because it survived block of AMPA and NMDA receptors with bath application of 6-cyano-7-nitroquinoxaline-2,3-dione (CNQX; 20 μM) and DL-2-amino-5-phosphonovaleric acid (DL-APV; 50 μM; $n = 6$ slices). Block of glutamatergic excitatory postsynaptic potentials (EPSPs) resulted in both a block of the up state (see Sanchez-Vives and McCormick 2000) and a significant reduction in spontaneous activity during the down state. However, in 4 of 10 recorded layer V sites in CNQX/APV, significant spontaneous activity remained (Fig. 1, *B–D*), suggesting that at least some layer V pyramidal cells discharge spontaneously through intrinsic membrane mechanisms (e.g. see Wang and McCormick 1992). We used these and other (Sanchez-Vives and McCormick 2000) features of the slow oscillation as guide lines in the generation of our model of this activity.

Slow oscillation and wave propagation of network activity

In accordance with the experimental observations of Sanchez-Vives and McCormick (2000), neurons in our model show spontaneous activity as repetitive episodes of low-rate neuronal firing, separated by long-lasting silences of ~2.5 s (Fig. 2). The oscillation frequency is thus ~0.4 Hz. Activity patterns are organized spatially as synchronous waves that propagate from one site to neighboring sites, thus recruiting the whole network at each firing episode of the slow oscillation (Fig. 2*B*). Typically, the most active part of the network initiates the discharge at each cycle (in Fig. 2*B*, 3rd row from bottom), but the initiation site is not unique and varies from simulation trial to trial.

The membrane potential of modeled pyramidal neurons, as also seen in experiments, undergoes transitions between more depolarized states with higher spiking activity (up states) and more hyperpolarized states with virtually no spike discharges (down states; Fig. 2*C*). Slow oscillation of the membrane potential occurs in parallel with waxing and waning of the intracellular sodium concentration: $[Na^+]_i$ accumulates slowly due to spike-triggered sodium influx during the up state and decays by an extrusion process to the extracellular medium during the down state (Fig. 2, *C* and *D*). We will show that the slow $[Na^+]_i$ dynamics is critical to the generation of slow oscillations (see following text).

Because neurons are not identical in the heterogeneous net-

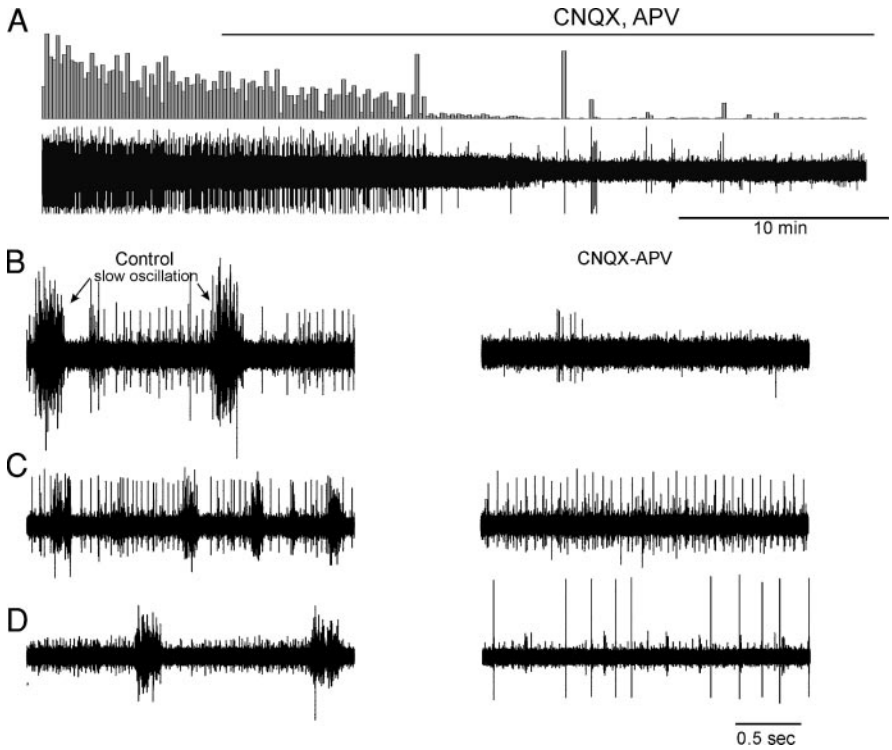

FIG. 1. Block of excitatory synaptic transmission eliminates the slow oscillation and reveals spontaneous action potential activity in a subset of layer V cells. *A*: extracellular multiple unit recording from layer V in prefrontal cortex during the bath application of 6-cyano-7-nitroquinoxalene-2,3-dione (CNQX, 20 μM) and DL-2-amino-5-phosphonovaleric acid (dl-APV, 50 μM). The slow oscillation (see expansion in *B*) is completely blocked and spontaneous discharge is greatly reduced. However, occasional action potential discharges still occur. *B*: expansion of recording in *A* prior (*left*) and following (*right*) block of excitatory synaptic transmission. *C*: recording at another site in layer V before and after block of excitatory transmission. *D*: another example of the slow oscillation recorded in control solution, and spontaneous activity recorded in a nearby site following the block of synaptic transmission.

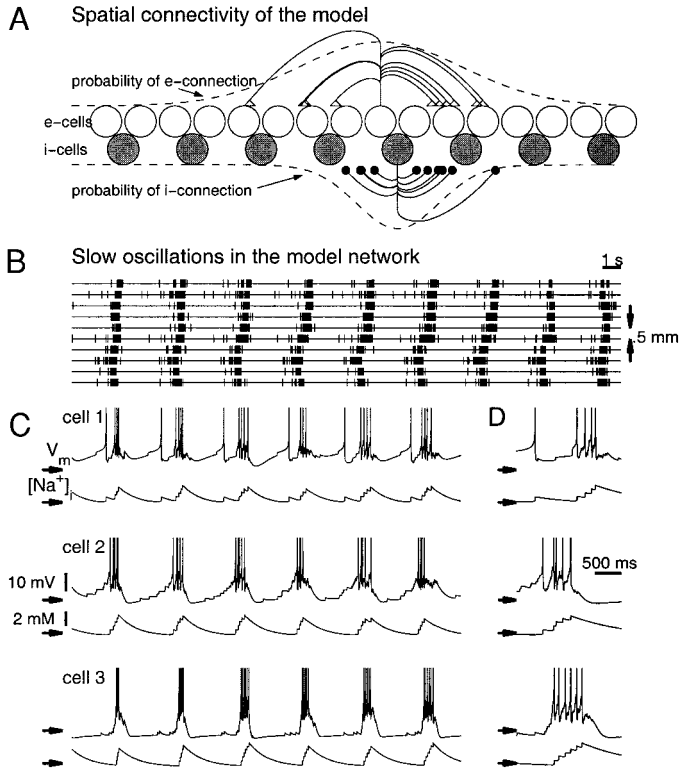

FIG. 2. The model reproduces spontaneous slow oscillations observed in the in vitro slice preparation. *A*: schematic representation of the spatial connectivity in the network model. A particular realization of the probabilistic connectivity for a pyramidal neuron and an interneuron is illustrated. - - -, probability distribution of synaptic connections from one neuron at the center to the rest of the network. Neurons are not drawn to scale with probability distributions. *B*: the spontaneous network activity can be visualized as multiunit recordings (5 neighboring cells per site, sites are spatially separated by 500 μm) to compare with the experiments of Sanchez-Vives and McCormick (2000). *C*: intracellular somatic voltage V_m and intracellular sodium concentration $[Na^+]_i$ of 3 representative pyramidal neurons. Calibration bars for central traces apply to all corresponding traces in *C* and *D*. Time scale as in *B*. *D*: blow-up of an individual depolarized episode of the cells in *C*. In *C* and *D*, $\rightarrow$s point at -75 mV for voltage traces and at 10 mM for internal sodium concentration.

work model, the membrane potential of pyramidal cells shows quantitatively different firing patterns. Some (highly excitable) cells show spike firing prior to the onset of an up state, and a relatively small after-hyperpolarization in the down state (Fig. 2, *C* and *D, top*). Other less excitable cells do not show spiking during the down state and have a pronounced and slowly recovering afterhyperpolarization following the firing discharge in the up state (Fig. 2, *C* and *D, middle*). And finally, a subpopulation of (the least excitable) pyramidal neurons exhibit clearly defined voltage up states and down states separated by $\sim$10 mV (Fig. 2, *C* and *D, bottom*). These differences arise from the random initialization of intrinsic properties for each cell, and, therefore, other neurons show intermediate behaviors between these three characteristic examples.

Propagating discharges can also be evoked by local external stimulation, for example by a brief depolarizing current injection to a subpopulation of 50 neurons (indicated by arrows in Fig. 3). Colliding waves usually merge and extinguish (3rd and 4th waves in Fig. 3*A*). The wave nature can be more clearly revealed when spontaneous activity is absent if all pyramidal cells are slightly hyperpolarized so that they are unable to trigger any network event by themselves. In this case, briefly stimulating by current injection a restricted area of the network triggers a discharge episode that travels across the network as a wave front (Fig. 3*B, left*) and merges with waves traveling in the opposite direction (Fig. 3*B, right*). Furthermore, stimulation immediately after an evoked discharge is unable to recruit the network for a renewed propagation (Fig. 3*B, left,* 2nd stimulation arrow). Experiments on the slice have yielded very similar results: external stimulation during the hyperpolarized phase of the oscillation generated a wave that propagated across the slice (Sanchez-Vives and McCormick 2000), and the slice was refractory immediately following one of these network events.

Model pyramidal neurons and interneurons fire in phase during the slow oscillation (Fig. 3, *A* and *B*). When pyramidal cells and interneurons at a given spatial location are closely examined, we found that interneurons typically discharge first in response to the arrival of the wave front (blue rim around activity in *B*, rightward shift in peak of histogram in *C*, and shift in average activity of pyramidal cells and interneurons in *D*). Pyramidal neurons have an average maximal rate of $\sim$10 Hz during the network discharge while interneurons fire at $\sim$20 Hz (Fig. 3*D*).

Change of input resistance during the slow oscillation

In Fig. 5 are plotted the time courses of synaptic and intrinsic ionic conductances in a pyramidal neuron during the slow oscillation. In particular, the input resistance of pyramidal neurons (here computed as the inverse of all open conductances across the membrane, see Fig. 4) is the highest during the down state, reaching its maximal value right before the onset of the discharge episode. The input resistance is at its minimum during the initial phase of the up state and increases gradually in the course of the up state (Fig. 5*B*). This is in agreement with experimental recordings during the occurrence of the slow oscillation in cortical cells of the anesthetized cat in vivo (Contreras et al. 1996). On the basis of this observation, Contreras et al. (1996) suggested that a K^+ conductance contributing to spike frequency adaptation cannot be responsible for the termination of the up state because this would lead to a gradual *reduction*, not increase, of the input resistance as the spike discharge progressed. This argument assumes that the K^+ conductance dominates the input resistance. In our model, the mechanism terminating the up state is the activation of a Na^+-activated K^+ conductance g_{KNa} (see following text). However, the input resistance is determined by the sum of all conductances and is dominated by the synaptic conductances rather than by g_{KNa}. During an up state, the slow activation of g_{KNa} produces spike-frequency adaptation; reduced neural firing leads to a decrease of recurrent synaptic conductances and other intrinsic ion conductances, hence an overall increase of the input resistance (Fig. 5, *C* and *D*).

Balance between synaptic excitation and inhibition

It is apparent in Fig. 5*C* that the excitatory and inhibitory synaptic conductances onto pyramidal neurons closely follow each other during the up state. This is shown more clearly in Fig. 6*A*, where the two synaptic conductances are not plotted against time, but against each other for seven different neurons

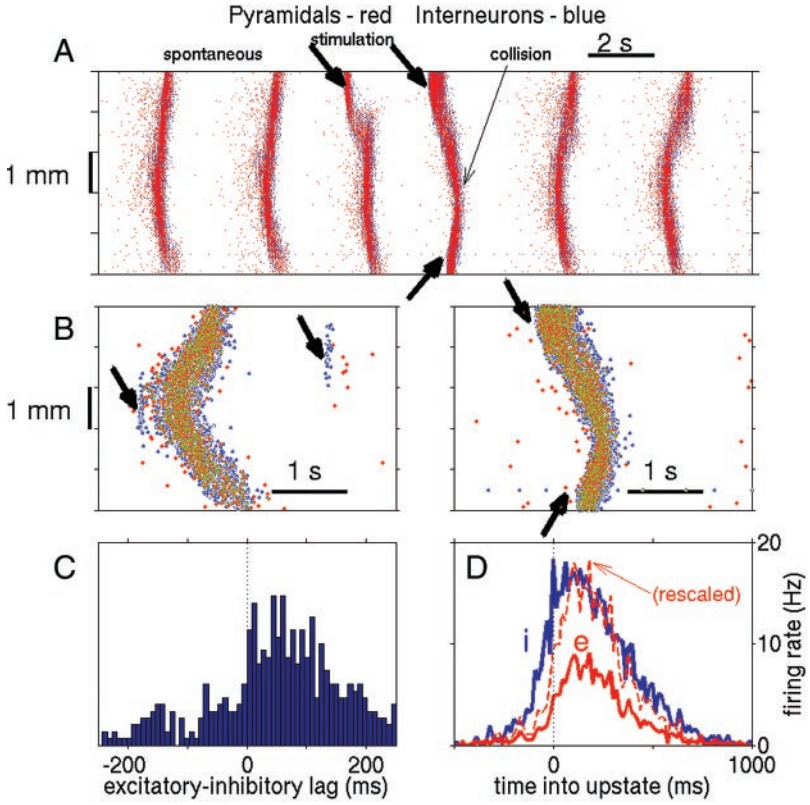

FIG. 3. Excitatory and inhibitory neurons fire in phase during the slow oscillation with interneurons typically firing before pyramidal neurons at the onset of the up state. *A*: rastergram of network activity during 20 s of simulation. Time is on the horizontal axis and the network is represented along the *y* axis. Each red dot corresponds to 1 spike at time *x* in the pyramidal cell located at position *y*. Blue dots are spikes fired by the inhibitory population and may be overlapped by red dots. Note spontaneously occurring discharges and evoked episodes (triggered by brief external stimulation indicated by tilted arrows). *B, left*: rastergram for an evoked discharge (brief external stimulation indicated by arrow) when pyramidal neurons are slightly hyperpolarized to prevent spontaneous oscillations. Where spikes from excitatory and inhibitory cells coincide in space and time, red and blue dots overlap and are illustrated as green. Note how the same external stimulation applied right after an evoked propagating wave fails to elicit a new discharge because of the refractoriness of the network. *Right*: example of a collision of 2 evoked waves. Note the faint blue rim (interneuron spikes) surrounding the wave in both panels, indicating that interneurons typically fire first and for a longer time during the up state. *C*: histogram of the intervals between the 1st spike of each pyramidal and its immediately adjacent interneuron in the time window shown in *B* (directly stimulated neurons are not shown). The histogram is biased toward positive time lags, indicating that on average interneuron firing leads pyramidal cell firing (by ~50 ms) at the onset of the slow oscillation discharge episode. *D*: firing rate averaged across neurons for the time window shown in *B*. Within the considered window, we substract from the spike times for each excitatory (inhibitory) neuron the time of the 1st spike of the closest lying inhibitory (excitatory) neuron, and then we construct the time histogram of those intervals in the red (blue) curve. Notice that interneurons firing leads pyramidal cell firing by ~50 ms, as also shown in *C*.

(*middle*), or averaged across 32 neurons equally spaced in the network (*right*). This plot yields a linear relationship, which means that the excitatory and inhibitory synaptic conductances increase and decrease in time in such a way that the ratio of the two g_{exc}:g_{inh} remains fixed. This ratio varies from neuron to neuron, ranging from 1:1 to 1:5. On average, inhibitory synaptic conductances are typically four times larger than excitatory synaptic conductances, g_{exc}:$g_{inh} \simeq 4$. Assuming that the average potential in the up state is about $\langle V \rangle = -55$ mV, the driving force for the excitatory current (with a reversal potential of $V_{exc} = 0$ mV) is $(V_{exc} - \langle V \rangle) \simeq 55$ mV, whereas that of the inhibitory current (with a reversal potential $V_{inh} = -70$ mV) is $(\langle V \rangle - V_{inh}) \simeq 15$ mV. Hence, the driving force for excitation is approximately four times larger than for inhibition. Therefore, an excitatory conductance four times smaller than the inhibitory conductance will yield comparable excitatory and inhibitory postsynaptic currents. In other words, there is an approximate balance between synaptic excitation and inhibition that is preserved over time throughout the up state, when pyramidal neural firing is sustained at relatively low rates (10 Hz).

To establish whether this excitation-inhibition balance is the result of a particularly well-tuned parameter choice or is an emergent property of the network, we drew the same graphs for network simulations where one synaptic conductance had been modified (Fig. 6, *B* and *C*). We observe that in all cases, the approximately linear relationship between excitatory and inhibitory conductances remains, but the proportionality ratio varies. It also becomes clear that the relationship is not exactly linear but follows a closed cycle, with excitatory conductances

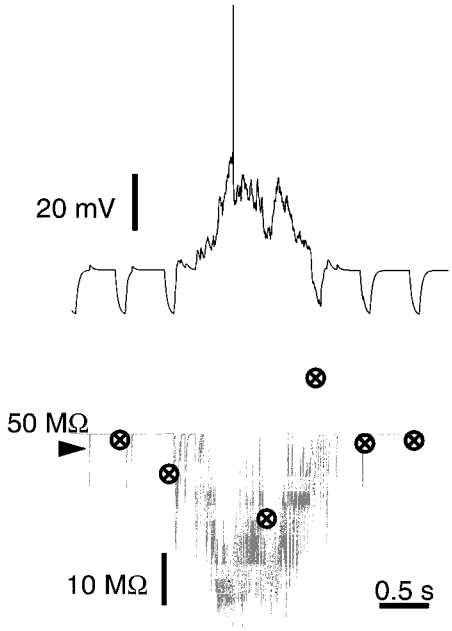

FIG. 4. Comparison between the input resistance calculated as the inverse of open membrane conductances in the model (gray plot in *bottom*) and that by the usual method employed in intracellular recordings through brief hyperpolarizing pulses (voltage trace in *top*, current pulses −0.3 nA, 100 ms). ⊗, the input resistances calculated as the ratio between the voltage deflection caused by each current pulse and the magnitude of the current (0.3 nA). Notice the quantitative agreement between the 2 estimates. The neuron was kept hyperpolarized (−0.25 nA) in the course of the network simulation to prevent spikes riding on the up state, which confounds R_{in} calculations with the pulse method.

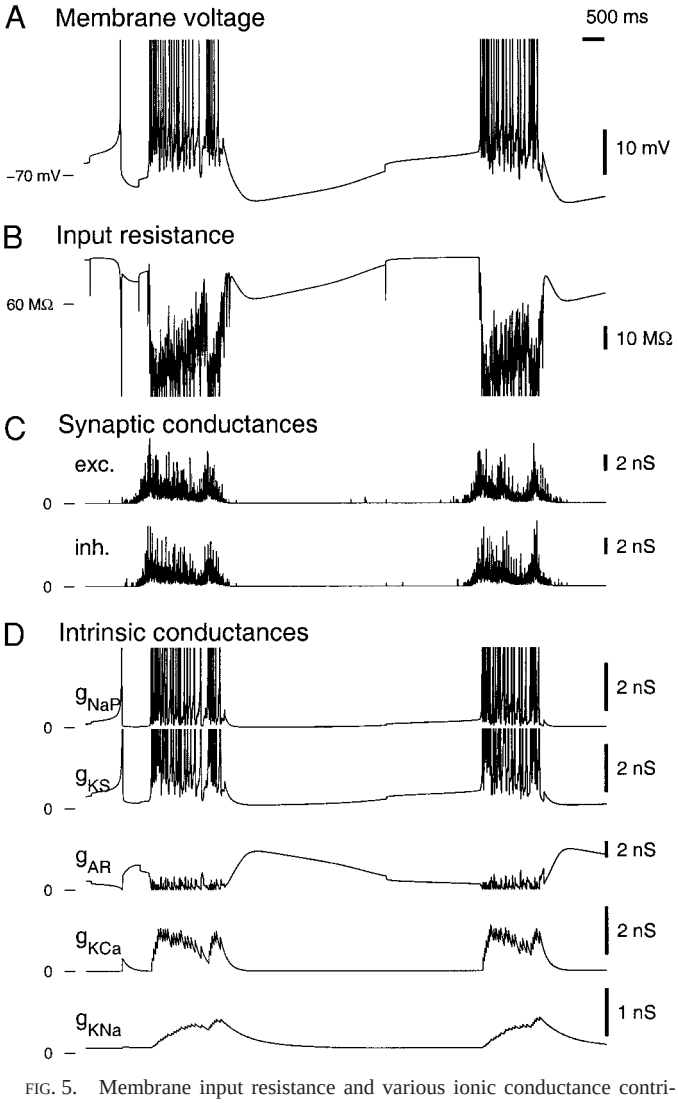

FIG. 5. Membrane input resistance and various ionic conductance contributions in the course of the slow oscillation. *A*: membrane voltage trace of 1 neuron while the network undergoes slow oscillations. *B*: total input resistance. Maximal resistance occurs right before the discharge onset and the resistance is minimal at the beginning of the up state. There is a gradual increase of the input resistance during the up state. *C*: excitatory and inhibitory synaptic conductances decrease as the discharge progresses. *D*: intrinsic conductances during the slow oscillation. g_{AR} is closed, while g_{KS} and g_{NaP} are activated, during the up state. Contributions from the other intrinsic channels, mostly from the passive leakage, are not shown but are included for input resistance calculation. Activity-dependent K^+ conductances (g_{KCa} and g_{KNa}) are weaker in magnitude (notice the scale on the *y* axis). For the sake of clarity, the data in this graph correspond to simulations with reduced g_{KNa} (g_{KNa} = 0.33 mS/cm^2), that have much longer up states. We have confirmed by performing averages over many neurons that the trends illustrated here hold true for the reference parameter set, such as that used in Figs. 2 and 3.

above (below) the average linear relationship during the down-up (up-down) transition (see Fig. 6*C*, *right*).

The exact ratio of excitatory to inhibitory conductances is likely to depend on other parameters like V_L. Indeed, in a much simplified model including only leak and synaptic currents, the membrane equation is $C_m dV/dt = -g_L(V - V_L) - g_E(V - V_E) - g_I(V - V_I)$. Assume that $V_E = 0$, $V_L = V_I = -75$ mV, and $g_L = 20$ nS. The steady state of the voltage is given by $V_{ss} = (g_L + g_I)V_L/(g_L + g_I + g_E)$. Then, the membrane potential could stabilize around its threshold even with an excitation-inhibition ratio of g_E:$g_I = 1$($V_{ss} \sim -56$ mV, if $g_E = g_I = 10$ nS). However, the issue of whether such a model could maintain its stability throughout a recurrently generated up state does not seem trivial because synaptic conductance increases proportional to the network activity could lead to reverberatory instability.

Mechanisms of the slow oscillation in the model

The basic mechanism for the emergence of the oscillatory activity in the network model is the interplay between neuronal spontaneous firing amplified by recurrent excitation, and a negative feedback due to slow activity-dependent K^+ currents. These positive and negative feedback processes operate along the lines illustrated in Fig 7: because the reversal potential of the leakage current is distributed randomly (see METHODS), some neurons are spontaneously active at very low rates (0.6 ± 0.2 Hz). Occasionally, a sufficient number of closely adjacent spontaneously active neurons fire together, thus triggering a cascade of recurrent excitation that locally brings the network into the firing regime of the oscillation (up state). At that point, activity-dependent K^+ currents (notably the Na^+-dependent K^+ current) start accumulating in active pyramidal neurons, reducing their excitability. The decremental excitability of pyramidal neurons eventually makes the network recurrence unable to sustain the firing state, and the local network reverts to the silent state via a slow afterhyperpolarization. The decay time of the currents responsible for this afterhyperpolarization sets the time scale for the reappearance of spontaneous firing and determines the periodicity of the oscillatory cycle.

According to this scheme, recurrent excitation should be responsible for quickly bringing neurons into the firing state in a collective manner, and the activity-dependent slow I_{KNa} eventually leads to a transition back to the down state. More specifically, we hypothesized that recurrent synaptic excitation produces a network bistability with an active up state and an inactive down state and that the slow kinetics of I_{KNa} drives the network to switch back and forth between these two states (see Fig. 8). We tested this prediction by substituting the time-varying I_{KNa} current with a constant hyperpolarizing current of varying intensities simultaneously in all model neurons. We found that the network indeed exhibits two stable dynamic states: the silent state with large hyperpolarization and the persistent firing state with low hyperpolarization. There is a range of current intensity over which these two states coexist (bistability; Fig. 8, *A* and *B*). In the control network simulation, the role of the injected hyperpolarizing current of Fig. 8 is fulfilled by the time-varying I_{KNa}, whose slow dynamics causes the neurons to cyclically trace this hysteresis loop (perimeter of shaded area in Fig. 8*B*): as I_{KNa} progressively builds up in the firing state (upper solid line in Fig. 8*B*), pyramidal neurons experience an increasing hyperpolarizing current. Eventually, point A in Fig. 8*B* is reached and neurons in the network collectively and sharply fall into the silent state because recurrent excitation is no longer sufficient to sustain their firing. Then neurons remain silent while I_{KNa} recovers slowly and the network regains the level of excitability (point B in Fig. 8*B*) where the silent state becomes unstable again and a collective sharp transition to the up state is generated. Thus the cycle goes on indefinitely, driven by the slow kinetics of I_{KNa}. Transitions between up and down states are sharp because of the sudden

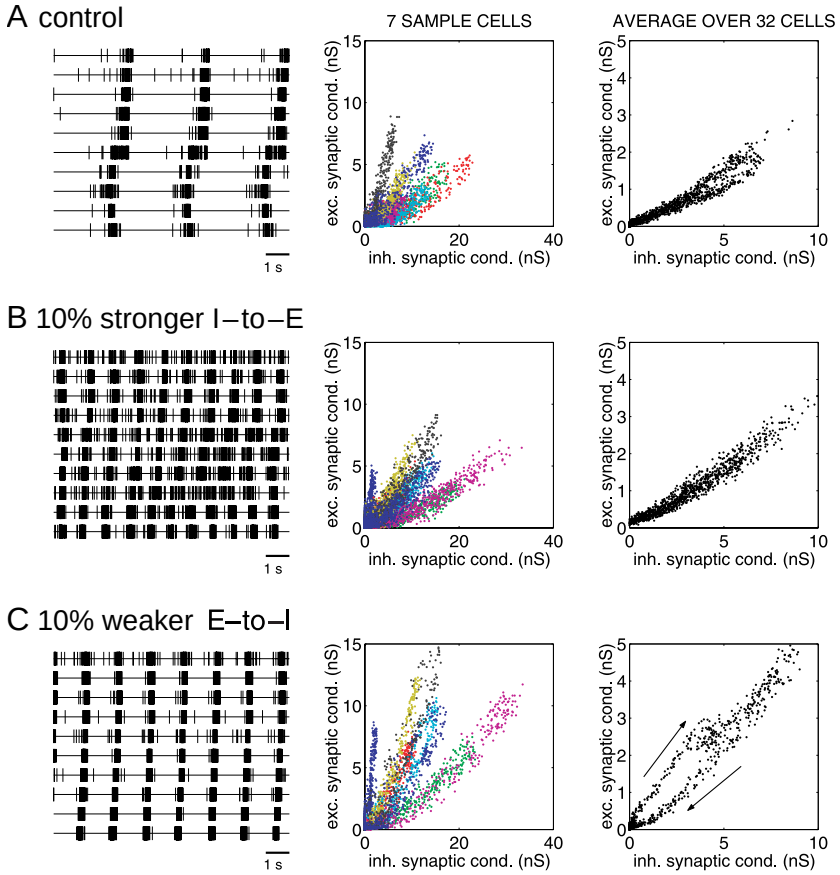

FIG. 6. Excitatory and inhibitory synaptic conductances preserve an approximate proportional relation to each other in the course of the slow oscillation. *A*: control network as in Fig. 2. *B*: same network with 10% enhanced inhibition to pyramidal neurons. *C*: network with 10% reduced excitation to interneurons. *Left*: network activity shown in a multiunit array record, distance between adjacent recording channels 0.5 mm. *Middle*: excitatory synaptic conductance plotted vs. inhibitory synaptic conductance for 7 different cells. Note the linear relationship between the 2 conductances, with the ratio (the slope of the linear plot) varying from neuron to neuron. *Right*: the excitatory and inhibitory conductances averaged across 32 neurons equally spaced in the network (calculated at each time step) and plotted against each other. The approximately linear relationship indicates that the balance between synaptic excitation and inhibition is maintained during the up state. Strictly, conductances do not keep an exact linear relationship but tend to depart systematically from it tracing an elongated closed cycle. This is especially evident in *C*, where arrows indicate the sense in which the cycle is traced in the course of the up state.

loss of network stability at a given degree of neuronal excitability.

To further test the importance of feedback excitation to the bistability phenomenon, we reduced the maximum conductance of the recurrent excitatory synapses to pyramidal neurons by 20%. The result is a loss of the bistable range (Fig. 8*C*). Now the network is either silent or, upon progressive depolarization of pyramidal neurons, it becomes spontaneously active. There is, however, no range of input currents for which both a quiescent state and a persistent firing state are simultaneously stable.

The mechanism for adaptation-induced network oscillations has been mathematically analyzed by van Vreeswijk and Hansel (2001) (see also Fuhrmann et al. 2002; Wang 1999b).

Pharmacological manipulations

To compare with the experimental results of Sanchez-Vives and McCormick (2000), we explored the effect of various synaptic receptor blockers on our slowly oscillating cortical network (Fig. 9). Blocking AMPAR-mediated transmission abolishes this rhythmic activity completely, and a subpopulation of excitable neurons fire spontaneously without any apparent network amplification. Similarly, the slow oscillation disappears under NMDARs blockade but this disruption is not as dramatic as when AMPARs are blocked, and occasional bursts of activity are able to recruit neighboring neurons into a network event via AMPAR-mediated transmission. On the

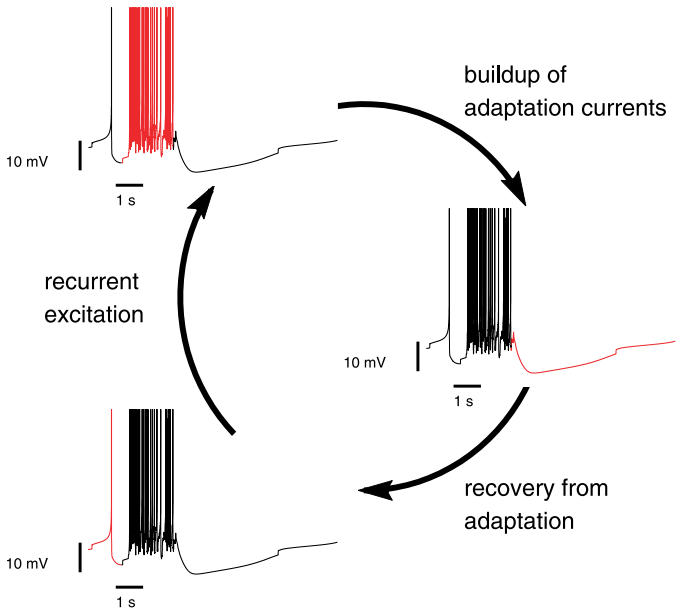

FIG. 7. Mechanism of the slow oscillation: some neurons have slightly lower spiking threshold and fire spontaneously (*bottom left*). This spontaneous firing will occasionally trigger the recruitment of all the cells in a subregion of the network through recurrent excitation and bring those cells up into the firing state (*top left*). While neurons fire, their activity-dependent K^+ currents (especially I_{KNa}) accumulate slowly. A point is reached in which the neurons are not excitable enough to maintain this self-sustained spiking state and they revert to the silent mode (*middle right*). Only after the Na^+-dependent K^+ current decays can the spontaneous firing resume and eventually trigger a new discharge episode (*bottom left*).

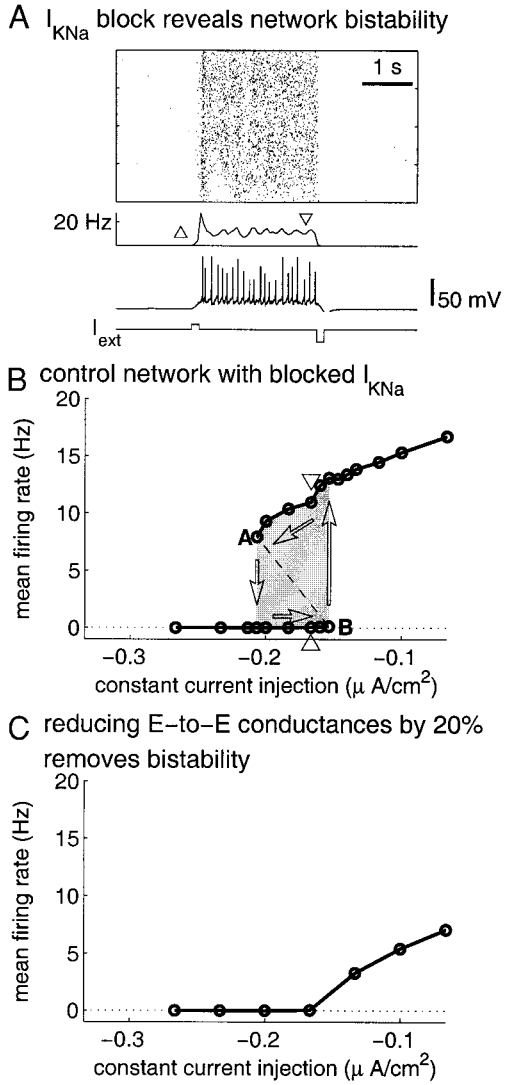

FIG. 8. Recurrent excitation produces network bistability for a range of values of the slowly decaying current I_{KNa}. The Na^+-dependent K^+ channel was blocked in all pyramidal cells, and a constant hyperpolarizing current I_{ext} was injected as a replacement in all of them. Simulations were repeated for a range of intensities of I_{ext} with the stimulation protocol illustrated in *A* (*bottom*): 2.5 s after the initiation of a simulation trial, a brief depolarizing pulse is injected into all pyramidal neurons, the network settles into a stable state for another 2.5 s, and then a brief hyperpolarizing pulse is injected. The average network firing rate is calculated before the depolarizing and hyperpolarizing pulses (triangles). The rastergram shows the network activity, where spikes are represented by dots at the firing time (along the *x* axis) and the position of the neuron on the network (along *y* axis). Below is the instantaneous population firing rate and a sample "intracellular" trace of one of the cells in the network. *B*: for a range of constant injected current (shaded area), the network can stably remain in the silent state or in a persistent firing state sustained by excitatory reverberation. Triangles correspond to the network firing rates in the example simulation of *A*, at the time points indicated by the same triangles. In the full model, the time-varying I_{KNa} plays the role of hyperpolarization current. When the neurons are in the sustained firing state, $[Na^+]_i$ slowly accumulates and the activation of I_{KNa} makes neurons move leftward along the upper branch of the graph (left-pointing arrow), up to the left end-point ('left-knee', point A) when the network abruptly drops down to the silent state. When neurons cease firing, $[Na^+]_i$ decays back to the baseline and I_{KNa} decreases slowly, so that neurons move rightward along the lower branch of the graph (right-pointing arrow), until they reach the right end-point ('right-knee', point B), when the network jumps back to the persistently firing state again. *C*: reducing excitatory feedback (E-to-E conductances) by 20% abolishes the network hysteresis, demonstrating that bistability requires strongly recurrent synaptic excitation.

other hand, blocking $GABA_A$Rs results in a more exuberant discharge that propagates at a much faster velocity across the cortical network. Also, the time intervals between burst episodes are significantly prolonged, i.e. the oscillation period is longer. All these behaviors are very similar to the results of Sanchez-Vives and McCormick (2000) after bath application of various synaptic receptor blockers in the slice preparation (compare the Fig. 9, *left* and *right*).

Velocity of wave propagation

Figure 9 shows that the network can sustain two different types of propagating waves depending on whether intracortical inhibition is functional (control case) or the network is disinhibited ($GABA_A$R block). Notably, these two waves have very different propagation speeds, as in slice experiments (Golomb and Amitai 1997; Sanchez-Vives and McCormick 2000; Wu et al. 2001). Both in the model and in the experiment, the propagation of the disinhibited wave is almost an order of magnitude faster than that of the wave in control conditions. The velocity of the disinhibited wave is largely determined by the efficacy of AMPAR-mediated excitatory synaptic transmission (Fig. 10*A*), consistent with previous analytical and simulation results (Ermentrout 1998a; Golomb and Amitai 1997). The dependence of the propagation speed on the strength of feedback inhibition is plotted in Fig. 10*B*. Either an increase of the inhibitory conductance onto excitatory cells or of the excitatory conductances onto inhibitory cells gradually decreases the wave propagation speed, according to a smooth sigmoid function (fitted curve).

Although the model reproduces roughly a 10-fold increase in the wave speed with inhibition blockade, a closer examination revealed that the absolute wave speeds in the model are significantly off the experimentally measured values. In control conditions, the velocity is <3 mm/s, whereas in the experiments it was $\sim$10 mm/s; with inhibition blockade, the wave propagation is <20 mm/s, when the experiment yielded a value $\sim$80 mm/s. We have explored possible solutions to this discrepancy. Figure 10*A* shows that with sufficiently strong E-to-E coupling, a wave velocity of $\sim$100 mm/s could be achieved in the disinhibited network. This suggests that one could first increase the strength of recurrent AMPA-mediated excitatory synapses to achieve the desired velocity in the disinhibited network; then, by gradually increasing the inhibitory feedback (as in Fig. 10*B*), slower propagation at a desired velocity could be obtained. However, this is not the case (Fig. 10*C*): with much stronger excitatory feedback (4-fold E-to-E AMPA conductances), increasing inhibition in a network does not lead to the slower propagation mode observed in the experiment. Instead, when the feedback inhibition is above a threshold value, the wave phenomenon disappears and the network shows a spatially uniform (unstructured) tonic firing state (shaded areas in Fig. 10*C*). Below this threshold but near it (inhibitory synapses are still very strong) a complex activity pattern emerges (see illustrative rastergram in Fig. 10*D*), in which activity propagates at two different velocities. The rastergram in a small time window reveals that activity spreads quickly, as in the disinhibited case ("fast wave" indicated in Fig. 10*D*). Examination at a longer timescale reveals also a slower propagation, which is nevertheless not a smooth wave-

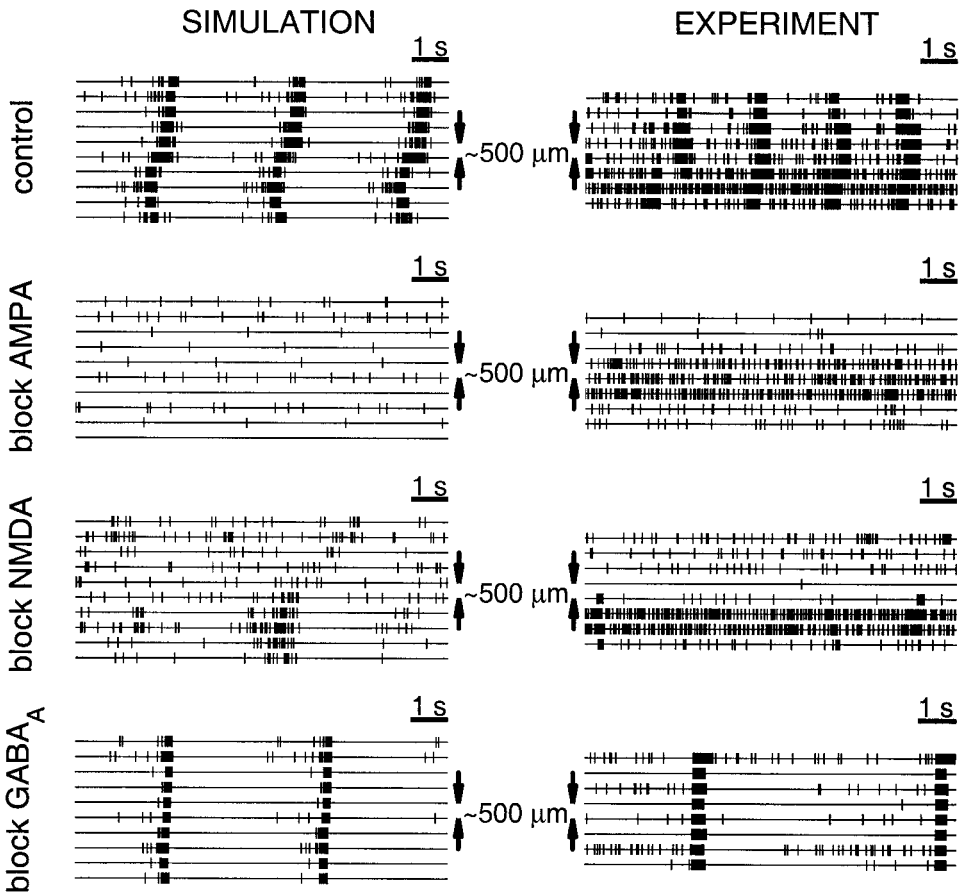

FIG. 9. Simulations with synaptic transmission blockade reproduce the experimental results. *Left*: simulation results plotted as multiunit records with blockade of the various synaptic receptors. *Right*: experimental results when CNQX, APV, or picrotoxin were applied in the bath solution of a slowly oscillating cortical slice. The experimental results shown as control correspond to the same slice as the results for *N*-methyl-D-aspartate (NMDA) blockade. Control traces are very similar (not shown) for the AMPA and $GABA_A$ blockade.

front ("slow propagation mode" indicated in Fig. 10*D*). The global network pattern is clearly not comparable to the one observed in the slice experiment of Sanchez-Vives and McCormick (2000).

Another possibility is to increase the spatial extent (the "footprint" σ_{EE}) of excitatory connectivity because the wave velocity increases proportionally with σ_{EE} (Ermentrout 1998b). However, to achieve the experimentally comparable wave velocities, one would have to increase σ_{EE} of the E-to-E coupling by three- to fourfold, from 250 μm (see METHODS) to ~2 mm, which would be inconsistent with the anatomical and physiological data. We examined the more plausible scenario that weak but long-range patchy horizontal connections could increase the propagation speeds significantly. This pattern of connection is prominent in the mammalian cortex (Gilbert and Wiesel 1983; Rockland 1985), and it has been observed in ferret visual cortex in both supragranular and infragranular layers (Rockland 1985). Typically, horseradish peroxidase injection in a restricted area of cortex results in orthograde striped staining of intracortical connections with stripe width of 250 μm and center-to-center distance 0.5–0.7 mm (Rockland 1985). We model this kind of connectivity as depicted in Fig. 11*A* (*right*). When we use this type of connectivity in our model, discharges propagate much faster in both conditions (Fig. 11*A*, *right* compare with *left* for non-patchy connectivity). For the wave in the disinhibited network, the velocity increased to >50 mm/s; whereas for the network with functional inhibition, the propagating wave has a speed close to 10 mm/s. On the other hand, the inclusion of long-range excitatory connections does not lead to a significant increase of the pyramidal neural activity, the firing rates are comparable to the situation without patchy excitatory connections. Both velocities depend markedly on the spatial extent and strength of the patchy horizontal connections (Fig. 11,*C* and *D*). Figure 11*C* shows how the center-to-center distance for the patchy horizontal connections influences the propagation speeds. The more separated the patches are spatially, the faster the wave propagates both in the control and disinhibited conditions. The firing rates of pyramidal cells decreased slightly as the waves became faster. In Fig. 11*D*, we show the dependency of the wave velocities on the strength of the lateral patches. The stronger the patched connections, the faster the wave. In this case, the firing rates grew slightly with the increase in excitatory patch strength.

Relative spatial range of excitatory and inhibitory projections

A still unresolved issue in functional cortical architecture is whether cortical inhibition has a larger or smaller spatial range than intracortical excitation. The spatial extent of a specific (e.g. interneuron-to-pyramid) connection depends on the convolution of the axonal projection from the presynaptic cells and the dendritic extent of the postsynaptic cells. Judging from the anatomical estimates of the axonal and dendritic spreads of cortical interneurons and pyramidal neurons (Lund and Wu 1997), one could argue that inhibition from most interneurons is likely to act more locally than excitation. However, there are

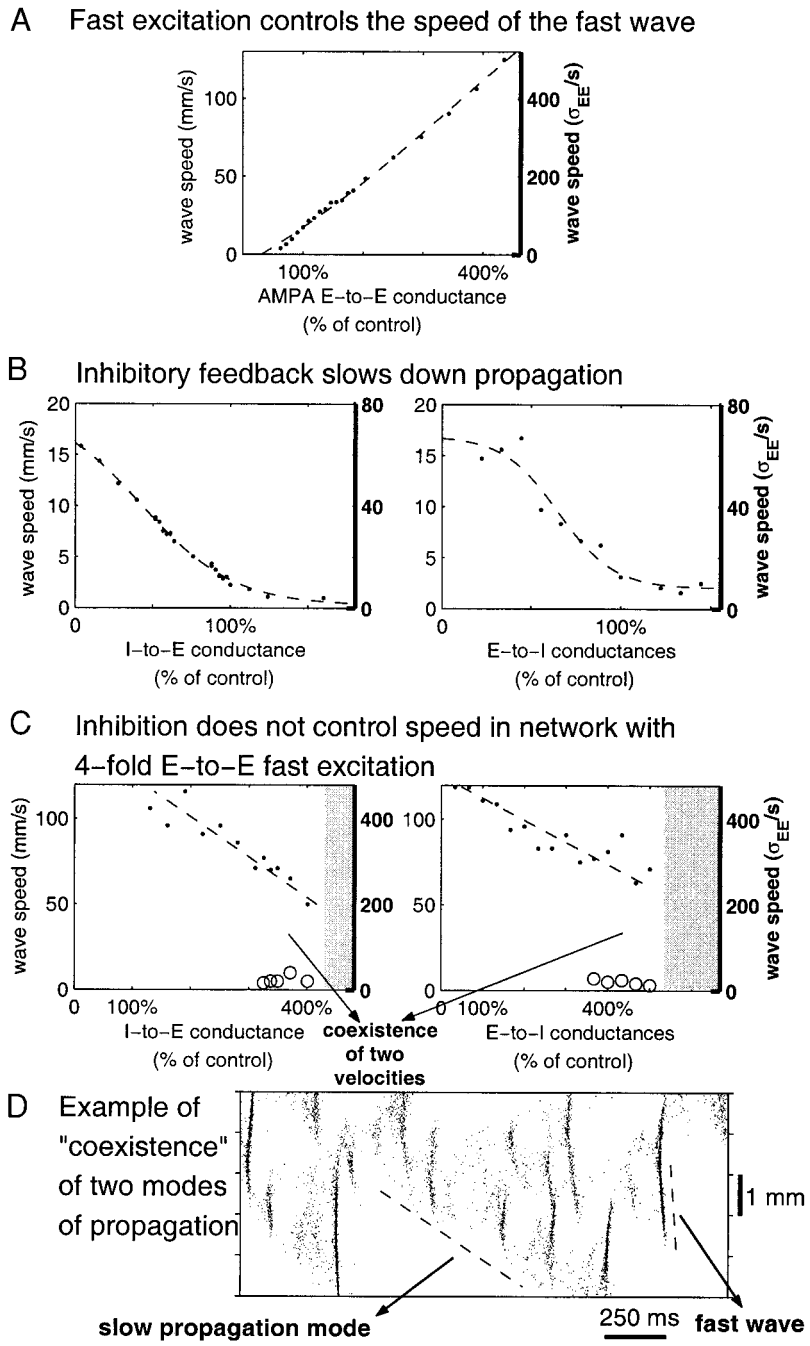

FIG. 10. Control of the propagation speed by recurrent excitation and by feedback inhibition. *A*: with inhibition blockade, the wave velocity increases linearly with the strength of fast recurrent excitation (AMPA E-to-E conductances on *x* axis, relative to the reference value). *B*: parametrical dependence of the wave velocity on the strength of feedback inhibition. *Left*: inhibitory conductance onto pyramidal neurons on *x* axis, relative to the reference value. *Right*: excitatory conductances (AMPA and NMDA) onto inhibitory neurons on *x* axis, relative to the reference value. *C*: setting AMPA-mediated E-to-E conductances 4-fold stronger yields correct propagation velocity in disinhibited networks (see *A*), but inhibition fails to control the wave to generate smooth slower propagation. Above a critical level (shaded area), the wave phenomenon is abolished and the network activity becomes spatially uniform. Below this critical value, the wave dynamics is complex: the network activity propagates at 2 distinct velocities (●, faster velocity; ○, slower velocity). *D*: example to illustrate the coexistence of 2 velocities of propagation in the network dynamics. The 2 distinct propagation velocities are indicated (- - -).

some classes of interneurons (e.g. a subset of cortical basket cells) with far-reaching axons (Buzás et al. 2001; Lund and Wu 1997) that could be functionally very powerful. Indeed, functional monosynaptic long-range inhibitory connections have been recorded electrophysiologically (Crook et al. 1998). We used our model to address whether one or the other scenario is more appropriate to reproduce the slow oscillatory activity observed in the cortex. To do that, we re-ran the network simulations with a broadened spatial width (footprint) of the inhibitory connection probability (from $\sigma_I = 125$ μm to $\sigma_I = 500$ μm), while keeping the footprint for excitation at $\sigma_E = 250$ μm. We still find very robust slow oscillations; the wave propagation velocity is ~5 mm/s (not shown).

Is there a way to distinguish these two cases ($\sigma_I/\sigma_E >$ or $<$ 1) experimentally? We focus on the temporal relationship between excitatory and inhibitory events as a possible discriminative test (Fig. 12). In both cases ($\sigma_I = 125$, 500 μm), interneurons tend to fire ahead of nearby pyramidal cells at the onset of the propagating discharge (Fig. 12, *A* and *B*). The relative timing of spike discharges in pyramidal cells and interneurons is therefore not a useful test for the functional significance of long-range inhibition. If the spread of the inhibitory axons is greater than the excitatory ones, then inhibitory synaptic conductances increase first in pyramidal neurons as the up state propagates through the network (Fig. 12, *C* and *D*). This is also shown in Fig. 12*G*, where simultaneous PSCs onto a pyramidal cell are shown under voltage clamp. If the spread of inhibitory connections is narrower than excitation

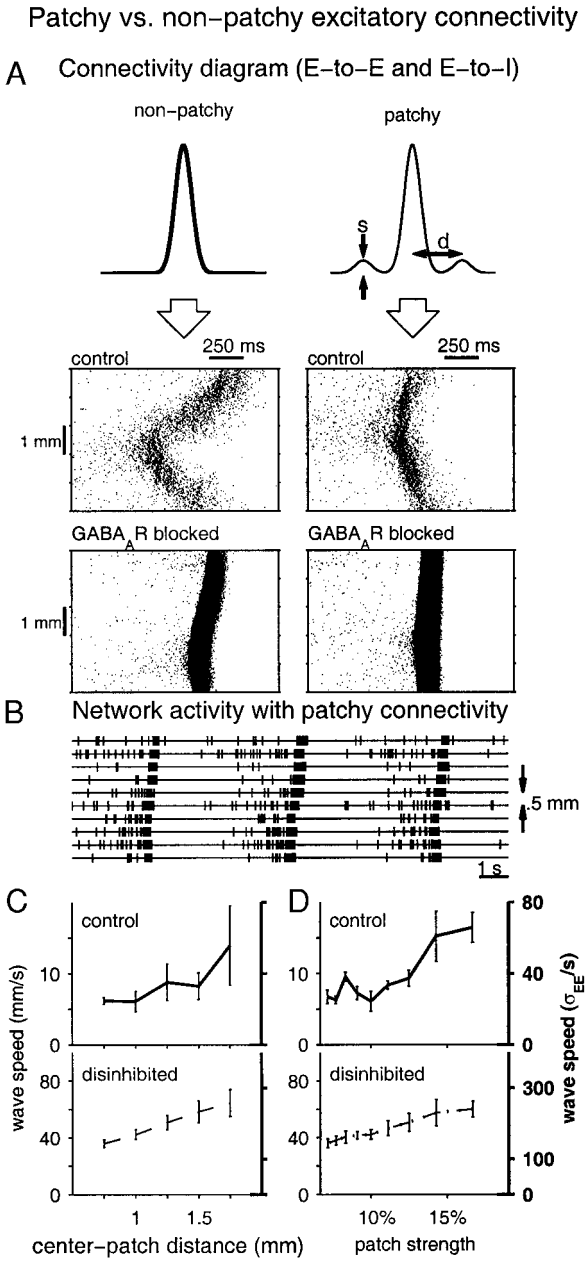

FIG. 11. Long-range patchy excitatory connections increase the velocities of wave propagation to be comparable to the experimental measurements, without dramatically increasing the firing rates. *A*: original excitatory probability distribution of synaptic contacts (*left*) and with the addition of the patchy connectivity (*right*). *Left rastergrams*: how the discharge propagates at 2 different velocities without patches with or without inhibition (control in *top*, $v \simeq 3$ mm/s; disinhibited network in *bottom*, $v \simeq 20$ mm/s). *Right rastergrams*: examples of wave propagation for a patchy excitatory connectivity with $d = 1$ mm and $s = 10\%$. *Top*: a wave in the network with functional inhibition ($v \simeq 8$ mm/s); *bottom*: shows the propagation of activity in the disinhibited case ($v \simeq 50$ mm/s). *B*: slow oscillation in the network model when patchy excitatory connections are included as seen with multiunit electrodes. The speeds of the propagating waves increase both with the center-to-center patch distance d (*C*, $s = 10\%$. *Top*: inhibited wave; *bottom*: disinhibited wave) and with the strength s of the lateral connectivity patches (*D*, $d = 1$ mm. *Top*: inhibited wave; *bottom*: disinhibited wave). In all graphs of *C* and *D*, left *y* axis labels absolute velocities with $\sigma_{EE} = 250$ μm and right *y* axis labels velocities in the unit of σ_{EE}/s.

(*left*), then the EPSCs and inhibitory PSCs (IPSCs) arrive to the pyramidal cells at approximately the same time. This occurs because, locally, interneurons fire in advance of excitatory

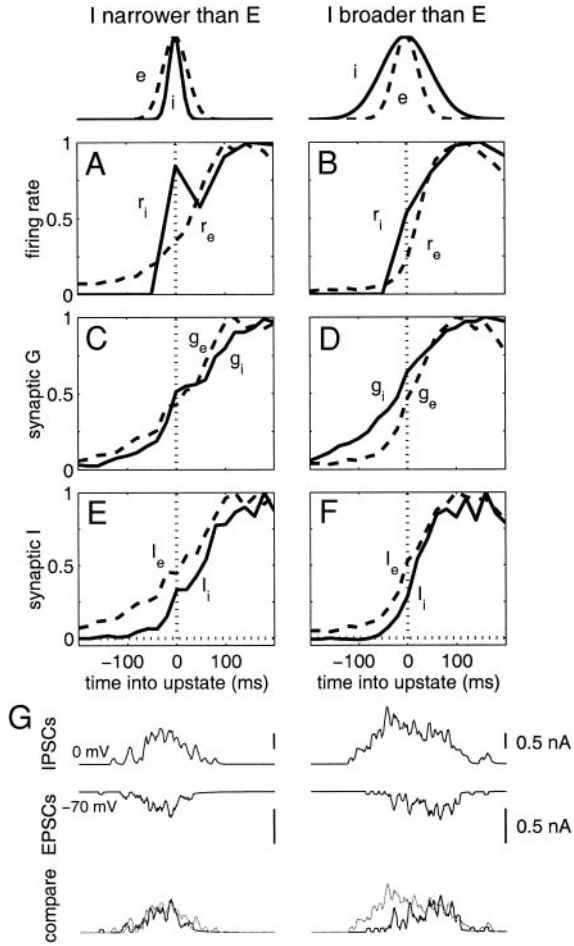

FIG. 12. The relative spatial range of inhibitory and excitatory synaptic connections only affects the time relationship between inhibitory and excitatory synaptic conductances but not the corresponding synaptic currents. Except for *G*, each curve is normalized by its maximal value. *Left*: reference parameter with narrower inhibitory connections (*top left*, —) than excitatory connections (*top left*, - - -). *Right*: modified parameter with broader inhibitory connections (*top right*, —) than excitatory projections (*top right*, - - -). The data show that in both cases inhibitory neurons tend to fire earlier than pyramidal cells (*A* and *B*, —: interneuron firing, maximum rate 24 and 38 Hz; - - -: pyramidal cell firing, maximum rate 10 and 18 Hz, respectively). The 2 synaptic conductances onto pyramidals rise at about the same time (*C*, —: inhibitory conductance onto pyramidals, maximum value 7.2 nS; - - -: excitatory conductance onto pyramidals, maximum value 2.2 nS). However, when inhibition has a longer spatial range than excitation, the inhibitory synaptic conductance leads the excitatory conductance (*D*, —: inhibitory conductance onto pyramidals, maximum value 9.5 nS; - - -: excitatory conductance onto pyramidals, maximum value 3.7 nS). What pyramidal neurons feel, though, is the synaptic current and in both cases excitatory and inhibitory synaptic currents start concurrently (*E* and *F*, —: inhibitory current onto pyramidals, maximum values 64 and 97 pA; - - -: excitatory currents onto pyramidals, maximum values 126 and 210 pA, respectively). This is due to the fact that an increased inhibitory conductance in the down state is purely shunting, and it does not participate in active inhibition until the neuron is depolarized by excitation. In each panel averages over different neurons ($n = 32$ and $n = 16$ in *left* and *right*, respectively) and various periods of the oscillation are computed, with *time 0* being set by the first spike in the propagating discharge of the nearest inhibitory neuron. *G*: single episode traces illustrating the relationship of inhibitory and excitatory postsynaptic currents (IPSCs and EPSCs) to each other in simulated voltage clamp recordings. In voltage clamp, synaptic currents are proportional to conductance changes and IPSCs are seen to lead EPSCs when inhibition is broader than excitation (see rescaled curves for comparison in lowest traces. gray, EPSCs; black, IPSCs).

cells. If the inhibitory connections are broader than excitation, then IPSCs precede the arrival of EPSCs (*right*). On the other hand, without voltage-clamp, during network oscillations, the synaptic currents that the neuron integrates in the course of the slow oscillation depend on the time-varying postsynaptic membrane potential $I_{syn} = g_{syn}(V - V_{syn})$. Figure 12, *E* and *F*, shows that this excitatory and inhibitory currents show similar time courses in both cases, with EPSCs slightly leading ahead of IPSCs. This is because initially the voltage is close to the inhibitory reversal potential, inhibition is purely shunting, and IPSCs become significant only after the cell is depolarized by EPSCs. As a result, PSPs measured in current clamp cannot be used to discriminate between long- and short-range inhibition unless the neuron is significantly depolarized away from the reversal potential of IPSPs.

These data suggest that the timing of EPSPs and IPSPs in intracellular recordings in slices may give clues as to the functional spread of inhibition and excitation in cortical networks. Recent experimental observations with intracellular recordings in layer V pyramidal cells during the generation of the slow oscillation in vitro demonstrate that the synaptic barrages are initially weighted toward excitation with a balance of excitation and inhibition being achieved over ~50–100 ms (Y. Shu, A. Hasenstaub, and D. A. McCormick, unpublished observations). In the view of the current model results, this would suggest that, functionally, the spread of inhibition has a narrower extent than that of excitation in the cortex.

Relation to in vivo slow oscillations under anesthesia

Slow oscillations observed in vivo can have distinct features depending on the particular experimental protocol. In contrast to the in vitro condition, up states can be longer than down states (Contreras et al. 1996; Cowan and Wilson 1994; Massimini and Amzica 2001; Stern et al. 1997; Timofeev et al. 2001), but in other cases the opposite occurs (Steriade et al. 1993b,c). In some cases, regular and robust slow oscillations are observed (Paré et al. 1998; Steriade et al. 1993b), whereas in other instances transitions between up and down states are irregular and stochastic (Cowan and Wilson 1994; Lampl et al. 1999; Paré et al. 1998; Stern et al. 1997). These marked differences between spontaneous cortical activity in vivo as seen by different laboratories may be due to the particular anesthetics protocol (kind and depth of anesthetics) used (Lampl et al. 1999). Since anesthetic agents often affect intrinsic neuronal excitability and synaptic transmission (Nicoll et al. 1990; Schulz and Macdonald 1981), we explored how a change in GABA or NMDA-mediated transmission or in the neuronal baseline excitability may affect spontaneous activity in our model network (Fig. 13). Neuronal intrinsic excitability was varied by modifying the leakage membrane permeability to K^+ ions (in the model this affects both the leak conductance g_L and the leak potential V_L). As leakage K^+ currents are progressively reduced, we observe that a sample neuron in the model goes from very stereotyped pronounced slow oscillations with short up states and long down states (Fig. 13*C*) to

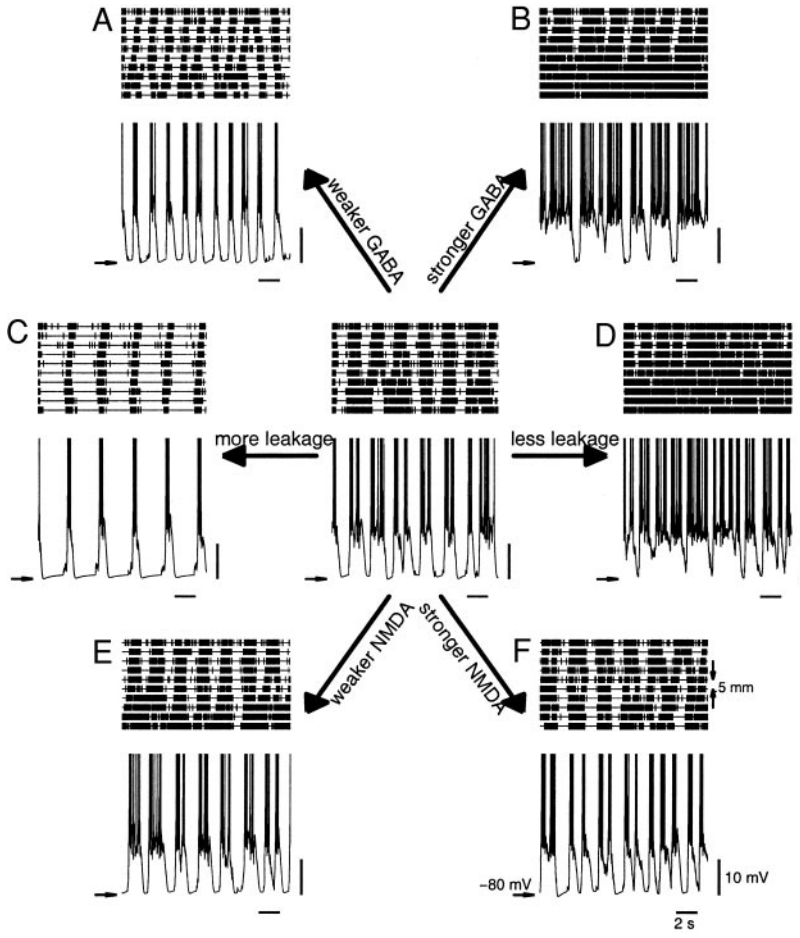

FIG. 13. Dependence of spontaneous cortical activity, as regular oscillations or irregular switchings between two stable voltages, on modulations associated with anesthetic agents. The same neuron was monitored in a model network as network parameters were varied from the reference case of Fig. 15*B* (central panel). All GABA conductances were modified by 10% (reduced in *A*, increased in *B*, as indicated). Intrinsic excitability was modified by changing the leakage K^+ permeability by 3% up (*C*) or 2% down (*D*), thereby modifying both the leakage conductance and the leak reversal potential. NMDAR-mediated transmission was modulated by 50% (reduced in *E*, increased in *F*). Top panels show the network activity pattern (as an array of multiunit channels) in each of these conditions.

fluctuations between a down state and an up state of more irregular durations (Fig. 13, center) and eventually to long sojourns in the up state and only occasional and brief incursions into the down state (Fig. 13*D*). Notice that Fig. 13*C* resembles the very rhythmic recordings by Steriade et al. (1993b,c); the center panel in Fig. 13 is reminiscent of the irregular traces in Cowan and Wilson (1994) and in Stern et al. (1997); and Fig. 13*D* simulates closely the data dominated by tonic-firing of Lampl et al. (1999), Contreras et al. (1996), and Timofeev et al. (2001). Synaptic modifications associated with anesthetic action on GABA channels could also induce changes in the pattern of network activity: enhanced inhibition made the slow oscillation more irregular (Fig. 13*B*) while reduced inhibition turned it more regular and faster (Fig. 13*A*). In contrast, NMDAR-mediated transmission modulation did not produce significant change in the oscillatory pattern of the network (Fig. 13 *E* and *F*). It may thus appear that the combined action of barbiturates via reduced neuronal intrinsic excitability and via the augmentation of GABA responses could compensate each other and have little effect on the pattern of slowly oscillating activity. Our simulations, however, show that reduced intrinsic excitability determines the overall activity pattern even when GABA responses are simultaneously enhanced (data not shown).

Therefore our model suggests that anesthetics-dependent changes in the network excitability, most notably through neuronal intrinsic excitability, may explain the various slow oscillating patterns, such as the durations of the up and down states and the statistics of transitions between the two states observed under different anesthesia protocols in vivo.

Transition to the tonic-firing state of vigilance

In unanesthetized cats, local field potential during quiet sleep shows slow oscillations (Timofeev et al. 2001); whereas the waking state is characterized by tonic-firing of spikes (Evarts 1964; Hubel 1959; Steriade et al. 1974) and fast oscillations in the local field potentials (Destexhe et al. 1999; Steriade et al. 1996; Timofeev et al. 2001). We used our network model, calibrated to reproduce the slice results, to simulate the transition from the slow wave sleep to the waking state with neuronal activity patterns observed from unanesthetized animals. It is well established that the transition from sleep to wakefulness depends critically on the activation of ascendent activating systems (especially cholinergic, noradrenergic, and serotoninergic), notably through an increased cholinergic input to the cerebral cortex (McCormick 1992; Steriade and McCarley 1990). We focused on manipulations that have been linked to neuromodulatory action by acetylcholine (see DISCUSSION): reduction of passive, activity- and voltage-dependent K^+ conductances, and reduced excitatory transmission (via presynaptic inhibition, see DISCUSSION).

We have considered various manipulations, each in isolation, to see whether any of them was in itself sufficient to simulate the transition to waking in terms of voltage traces and input resistance. We found that when Na^+-dependent K^+ conductance alone was significantly reduced, the network reverted to activity with less marked periodicity, longer up states and shorter down states (see Fig. 14*A*, *middle*). Further reduction of this adaptation current led the network to a tonic firing mode with no global spatiotemporal coherence (but still some weak

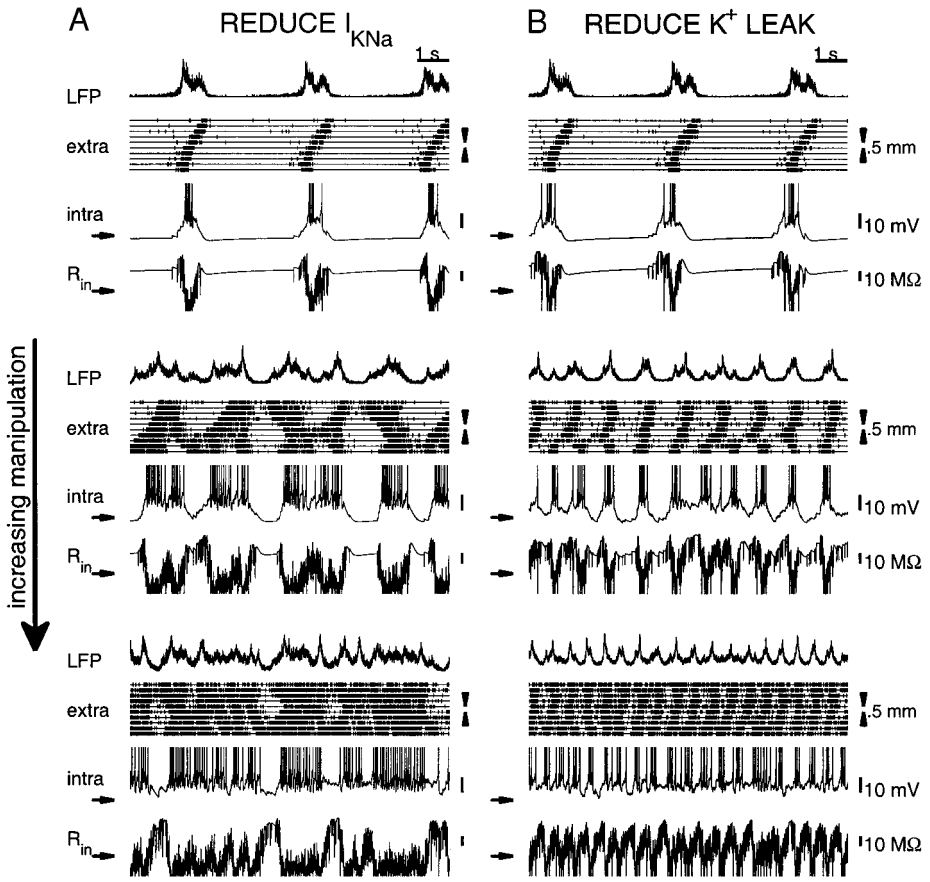

FIG. 14. Various manipulations bring the model network from the slow wave state and tonic activity state, similar to the transition between sleep and waking states of the brain. Each column shows 3 illustrative panels of increasing degrees of the parameter manipulation indicated in the column titles. Each illustrative panel includes: local field potential (LFP, calculated as the average synaptic activity over the whole network and normalized to the standard deviation of the resulting signal), population activity in multiunit electrode representation and membrane voltage trace and input resistance for a selected neuron. *A*: gradual reduction of the Na^+-dependent K^+ current (I_{KNa}) brings the network from a slowly regularly oscillating regime (*top*, parameters as described in METHODS) into a more irregular and faster oscillation (*middle*, $g_{KNa} = 0.27$ mS/cm^2) and eventually to a non-oscillating tonic-firing state (*bottom*, $g_{KNa} = 0.13$ mS/cm^2). *B*: progressive reduction in leakage K^+ permeability of pyramidals also changes from regular slow oscillations (*top*, as in *A*, *top*), to somewhat faster oscillations (*middle*, $g_L = 0.067$ mS/cm^2, $V_L = -60.84$ mV) and to tonic firing (*bottom*, $g_L = 0.06$ mS/cm^2, $V_L = -56.23$ mV). As shown experimentally, all of these effects could be attributable to the action of acetylcholine on cortical circuits. In all panels, arrows point at a voltage of −75 mV or at an input resistance of 40 MΩ.

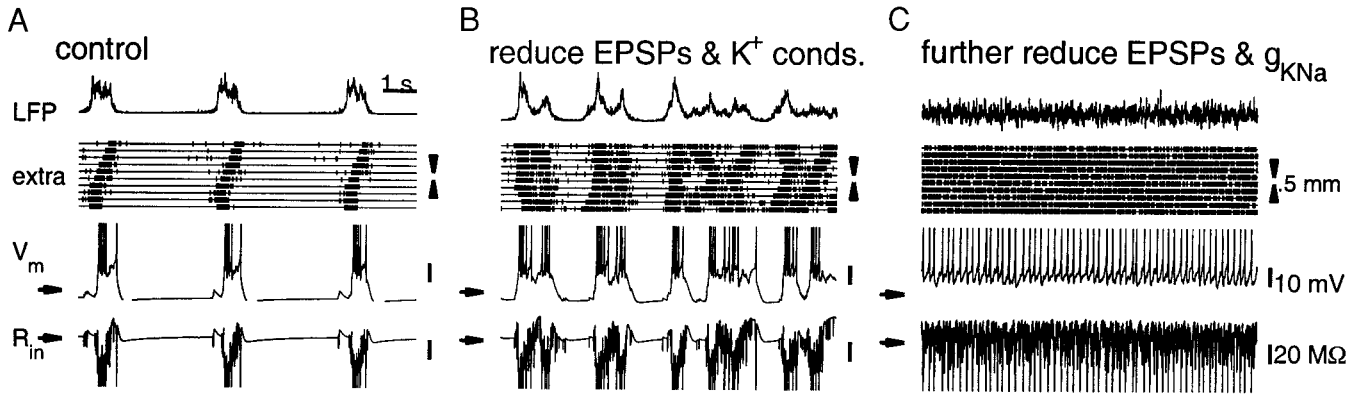

FIG. 15. The model network can show spontaneous activity corresponding to various states of vigilance of the brain. *A*: local field potential (LFP), population activity in multiunit electrode representation and a single neuron's membrane potential and input resistance for a slowly oscillating network (parameters as in Fig. 2 but with interneurons leakage currents given by $g_L = 0.104 \pm 0.0025$ mS/cm^2 and $V_L = -64.2 \pm 0.15$ mV). Activity as in the slice preparation or in some instances of anesthetized animals (Steriade et al. 1993b,c). *B*: same data for a network in which Na^+-dependent adaptation currents have been reduced by 25%, g_{KCa} by 25%, g_A and g_{KS} by 5%, g_L by 3% (and V_L was depolarized by 1.2 mV), AMPAR-mediated transmission by 10% and NMDAR-mediated transmission by 30%. As seen experimentally, all of these effects could be attributable to the action of acetylcholine on cortical circuits. Notice longer up states of more irregular duration, similar as seen during slow-wave sleep in unanesthetized cats (Timofeev et al. 2001). *C*: same as in *B* with AMPAR-mediated transmission further reduced by 33%, NMDAR-mediated transmission by 30% and g_{KNa} by 33%. Oscillations disappear and LFP becomes flat, as occurs during the waking state. Mean rates averaged across the network are 1.3 Hz (*A*), 4.8 Hz (*B*), and 5.5 Hz (*C*). Notice that rates do not increase significantly from *B* to *C*, as observed in the transition between slow-wave sleep and waking. In all panels, arrows point at a voltage of -75 mV or an input resistance of 60 MΩ.

faster oscillations are to be seen in the local field potential at ca. 2–3 Hz), the voltage traces are thus reminiscent of those characteristic of the "waking state" (compare to data in Steriade et al. 2001; Timofeev et al. 2001). Other aspects, however, indicate that adaptation current reduction is not the only ingredient of neuromodulatory action important for the "waking up" of the circuit. In particular, the overall firing rate of the network increases in the process (from 1 Hz in the *top* and 5 Hz in the middle panel, to 9 Hz in the *bottom* of Fig. 14*A*), and the input resistance of the neuron is significantly reduced. This is in contrast to experimental observations (Steriade et al. 2001) that indicate that the overall firing rate of neurons remains approximately the same between the natural slow oscillation and the waking state, even though during the up state of the slow oscillation the apparent input resistance is lower.

On the other hand, the reduction of leakage K^+ permeability (reduced g_L and increased V_L) in pyramidal neurons also affects the transition from a slowly oscillating network into tonically firing neurons (Fig. 14*B*). With this mechanism, as also observed when reducing I_{KNa}, the overall firing rate also increases considerably (from 1 Hz in the *top* and 4 Hz in the *middle* to 8 Hz in the *bottom*), and the input resistance decreases (presumably due to enhanced synaptic conductance), contrary to the experimental evidence. The last mechanism that we examined is the reduction of intracortical excitation to pyramidal neurons (not shown). The effect is also to transform a slowly oscillating network into tonic activity, the difference with the previous mechanisms is that this tonic firing is now extremely sparse at very low rates (0.2 Hz) and does not look comparable to intracellular recordings during the waking state. Trivially, however, input resistance increases because of the practical absence of synaptic activity.

When these effects of the neuromodulatory action are combined in the network model (Fig. 15), the reduction of recurrent excitatory synaptic conductances leads to an increase in the input resistance, whereas the decreased excitation is compensated by the reduction of K^+ currents so that the firing rate in the tonic state remains comparable to that in the up state of the slow oscillation mode. Therefore a transition from the slow oscillation state characteristic of natural sleep to the tonic firing state of the waking state is realized, with neural activity and input resistance changes consistent with the experimental observations (Steriade et al. 2001).

DISCUSSION

Cellular and network mechanisms of the slow (<1 Hz) oscillation

In this paper, we present a model that reproduces the slow rhythmic activity (<1 Hz) observed in vitro by Sanchez-Vives and McCormick (2000) and in vivo by Steriade et al. (1993b). The network oscillates between an up state of sustained but low-rate (~10 Hz) neural activity and a down state of membrane hyperpolarization. The onset and maintenance of the active up state is due to an amplification of spontaneous activity by powerful recurrent excitation, whereas the transition back to the down state is controlled by a slow negative feedback, the Na^+-dependent K^+ current I_{KNa}. We provide experimental evidence that when excitatory glutamatergic transmissions mediated by AMPA and NMDA receptors were blocked, a subset of layer 5 neurons still displayed significant spontaneous activities. Our model suggests that such spike discharges of single neurons are sufficient to trigger waves of activity that propagate across the cortical tissue. This initiation mechanism is in contrast to that of spike-independent spontaneous synaptic transmission proposed by Timofeev et al. (2000a).

Our results are in support of the hypothesis that the up state is sustained by local reverberatory circuits in the cortex (Contreras et al. 1996; Metherate and Ashe 1993; Sanchez-Vives and McCormick 2000). More specifically, our model proposes

that this oscillatory activity is the signature of an intrinsic bistability between the up and down state and that I_{KNa} induces slow switchings between these two states. One testable prediction of this scenario is that if I_{KNa} could be suppressed, for example by neuromodulators such as acetylcholine or norepinephrine, the local cortical network would become bistable, where both the up and down states would be dynamically stable. In that case, transient stimulation would set the network into a self-sustained (up) firing state, whereas transient hyperpolarization would revert it back to the silent (down) state. Moreover, this bistability would depend on strong excitatory reverberation and should disappear with reduced recurrent excitation. Finally, in the presence of I_{KNa}, the cortical slice is predicted to cycle around the bistability loop as depicted in Fig. 8 during the slow oscillation.

The ability of a cortical module to sustain several stable states of firing has been proposed as a possible mechanism for working memory in association cortical circuits, especially the prefrontal cortex (Compte et al. 2000; Wang 1999b, 2001). Our findings hint at the potential existence of a bistable dynamics in the primary visual cortex that could be made available operationally by reducing slow adaptation currents or enhancing after-depolarizing currents via neuromodulators (McCormick 1992). We emphasize that such a bistability has not yet been demonstrated experimentally and thus represents a testable prediction of our model. It is also important to note two major differences between the kind of bistability discussed here and that required for working memory. First, for a working memory circuit, a persistent up state should be stimulus-selective and involve only a subset of neurons (a neural assembly). By contrast, the up state during slow oscillation is global and recruits the entire network. Second, bistability of a working memory network would be between a resting state of spontaneous activity (at a few Hz) and a persistent active state with elevated firing rates (20–50 Hz). On the other hand, the bistability associated with slow oscillation is between a down state of membrane hyperpolarization and an up state of relative low firing rates (at $<$10 Hz). As the network is transformed from the slow oscillation mode to the tonic-firing mode, the persistent up state is similar to the spontaneous state of wakefulness (at $\leq$10 Hz) (Destexhe et al. 1999; Steriade et al. 1996), rather than higher-rate mnemonic activity states.

Input resistance and neuronal versus synaptic adaptation

Contreras et al. (1996) found that during the slow oscillation, the input resistance is at its lowest of the cycle at the beginning of the depolarized state and then it increases until it reaches its maximum at the end of the hyperpolarized phase of the oscillation. This was interpreted as evidence that the primary cause for the sudden transition to the silent down state was the depression or "disfacilitation" of an excitatory synaptic current as opposed to the accumulation of an activity-dependent hyperpolarizing current. The short-term synaptic depression mechanism has been implemented in a network model of the slow oscillations as they occur in deafferented cortical slabs (Bazhenov et al. 2002; Timofeev et al. 2000a). Presumably, that model is also endowed with an intrinsic bistability, and the network cycles around the hysteresis loop by the slow dynamics of synaptic depression in a similar manner to that described in Tabak et al. (2000).

We have built our model based on the experimental evidence that a Na^+-dependent K^+ current plays a critical role in the slow oscillation in vitro (Sanchez-Vives and McCormick 2000). Our model shows that I_{KNa} can be responsible for the termination of the up state firing, whereas the input resistance has the same time course as observed experimentally. This is because an increase in I_{KNa} results in decreased firing and reduced synaptic and voltage-dependent conductances. Whether the input resistance increases or decreases will then depend on the particular balance between the opening of the adaptation conductances and the closing of synaptic conductances (resulting from reduced activity in the network). Our model suggests that the increase of input resistance in the course of the up state is indeed primarily due to a decrease of the synaptic conductances, but this decrease could arise as an indirect consequence of intrinsic spike-frequency adaptation rather than a direct synaptic depression. Moreover, the inhibitory conductance g_I shows a much larger change than the excitatory conductance g_E, hence dominates the overall input resistance.

Interestingly, during slow oscillations, we found that g_E and g_I co-vary in such a way that the ratio g_I/g_E remains roughly fixed in time, so that the two synaptic currents (conductance times the driving force) are about the same. This dynamic balance of synaptic excitation and inhibition, as well as intrinsic potassium currents (such as the low-threshold I_{KS}) (Nisenbaum et al. 1994; Wilson 1992), contribute to the control of low firing rates ($\leq$10 Hz) in the up state and avoid the generation of runaway excitation.

Propagation of neural activity and the wave velocity

A number of previous theoretical works have been devoted to the understanding of the velocity of wave propagation in a one-population of pyramidal neurons, corresponding to slice preparations with inhibition blockade (Bressloff 2000; Ermentrout 1998b; Osan et al. 2002). In particular, this topic was experimentally surveyed and theoretically modeled by Golomb and Amitai (1997). They found that discharges propagated as traveling pulses in the disinhibited slice, propagation was possible only above a threshold value for the AMPAR conductance (g_{EE}^{AMPA}) and beyond that point the propagation velocity increased linearly with g_{EE}^{AMPA}. All these points have been reproduced by our model (see Fig. 10*A*). They further showed that NMDA receptor conductance had a much smaller effect on the discharge propagation, as our model also confirmed (data not shown).

More recently, Golomb and Ermentrout (2001, 2002) extended the analysis to a model with two (excitatory and inhibitory) neural populations of leaky integrate-and-fire neurons. They found that two wave propagation modes existed with very different speeds, and they predicted that in the slow wave inhibitory neuron firing would precede the pyramidal cell discharge. This is precisely what our more detailed model shows, thus confirming their prediction. Interestingly, within the range of parameters that we examined, interneurons always fire in advance of pyramidal cells at the onset of an up state, regardless of whether the inhibitory projection is narrower or broader than excitation. This prediction could be checked experimentally by comparing the firing times of intracellularly recorded pairs of a pyramidal cell and an interneuron at the same

recording site or by comparing the discharge of pyramidal cells and interneurons at the same site to a common reference, such as multiple unit or local field potential activity. Golomb and Ermentrout (2001) also found that the network could be in a regime where both modes of propagation occurred, depending on the way in which the network was stimulated. We did not explicitly find this situation in our network. However, it is conceivable that this behavior could be observed with the appropriate parameter modification.

In Golomb and Ermentrout (2001, 2002), the propagation of a wavefront was considered with the constraint that each cell is allowed to fire only one spike. By contrast, our model reproduces both the wave propagation of the onset of a long-lasting up active state and the slow oscillation between the up state and down state. We found that with anatomically estimated spatial ranges of synaptic connections, it is difficult to reproduce quantitatively the measured velocities of wave propagation. Typically the wave speeds in the model are three- and fourfold lower than the experimental data. It is not straightforward to obtain larger wave speeds by increasing excitatory synaptic conductances because the latter lead to complex firing patterns and high neural firing rates in the up state incompatible with the observations. On the other hand, by introducing weak long-range intracortical excitation, these connections are effective at recruiting neurons during the firing phase of the oscillation in such a way that they mediate faster discharge propagation. Our model predicts a strong relationship between the wave velocity observed physiologically and the inter-patch distance of long-range horizontal connections measured anatomically, which can be tested experimentally. The recruitment of long-range connections during cortical spontaneous activity has also been suggested to operate in anesthetized preparations in vivo (Tsodyks et al. 1999).

In our model, whether the inhibitory connections are narrower or broader than the excitatory ones is not crucial for the generation of slow oscillations. In either case, the model can generate slow propagating waves. These two scenarios of intracortical connectivity cannot be distinguished based upon the relative timing of activity in nearby inhibitory and excitatory neurons but only by examining in voltage-clamp the relative timing of EPSCs and IPSCs that arrive in pyramidal cells in the transition to the up state. We predict that inhibition should arrive earlier than excitation in pyramidal cells if long-range inhibition is a significant ingredient of intracortical circuitry. If the cell is at or near the reversal potential for this inhibition, then this should appear as an initial increase in membrane conductance (shunt) without significant change in membrane potential.

Slow oscillations in vitro and in vivo

The spontaneous cortical activity recorded in in vivo preparations under urethan or ketamine-xylazine anesthesia is not always univocally identified as slow oscillations. In some instances, membrane voltage transitions between an up state and a down state can be quite unpredictable, and they are then classified as a fluctuating rather than an oscillating pattern (Lampl et al. 1999; Stern et al. 1997). The issue of the coherency of the activity of cortical neurons is also a matter of debate since some authors find very good correspondence between neuronal up states and EEG waves (Paré et al. 1998; Steriade et al. 1993c), but other experiments show poor coherence between individual neurons and EEG (Lampl et al. 1999). An obvious question is then how to reconcile all these various observations with the hypothesis that they are manifestations of one single phenomenon. Our network simulations provide a hint as to how these types of behavior could be related to each other. We found that an irregularly oscillating network (Fig. 13*B*) turns into a more periodic oscillation at a lower frequency (Fig. 13*A*) when the pyramidal neuron intrinsic excitability is reduced (by increasing permeability to K^+ ions through leakage channels). Also the inverse manipulations make the neuron spend more time in the up state and less in the down state (as in Fig. 13*C*). One of the anesthetic agents typically used in in vivo experiments is xylazine, which increases K^+ conductances through $\alpha 2$ noradrenergic receptors (Nicoll et al. 1990). For anesthetic effective concentrations, barbiturates also have a hyperpolarizing effect through a GABA-mimetic action (opening Cl^- channels) that occurs in parallel to an augmentation of GABA responses (Schulz and Macdonald 1981). Our model suggests that these variations in excitability and connectivity may explain the variations in the pattern of activity generated in cortical networks between the in vitro slice, anesthetized and naturally sleeping animal.

Transition to the tonic firing state of vigilance

In unanesthetized animals, the membrane potential of cortical pyramidal cells is characterized by transitions between an up and a down state in slow-wave sleep and a tonically depolarized state with firing at low rates during waking (when the animal's head is kept rigid) (Steriade et al. 1996, 2001; Timofeev et al. 2001). The average firing rate over long periods of time of a neuron is relatively similar over the sleep-waking cycle, and the input resistance of pyramidal cells in the waking state is as high as it is for the down state of the slow oscillation (whereas it is significantly lower for the up state of the slow oscillation) (Steriade et al. 2001).

Several neuromodulators are involved in the regulation of the brain's state of vigilance, including acetylcholine, norepinephrine, and serotonin (McCormick 1992; Steriade et al. 1997). Cholinergic modulation in cortical neurons is known to reduce several K^+ conductances: leak, A-type, M-type, and Ca^{2+}- and Na^+-dependent (Constanti and Sim 1987; Foehring et al. 1989; McCormick 1992; Schwindt et al. 1989). Another known effect of acetylcholine is the reduction via a presynaptic mechanism of EPSPs both in hippocampus (Hasselmo and Fehlau 2001; Seeger and Alzheimer 2001; Valentino and Dingledine 1981) and in neocortex (Kimura and Baughman 1997; Kimura et al. 1999; Tsodyks and Markram 1997). Kimura et al. (1999) have estimated that ACh suppresses $\leq$50% of intracortical synaptic excitation. On the other hand, serotonin also reduces these adaptation currents while diminishing the size of unitary EPSPs (McCormick 1992). These neuromodulators are likely to be at low levels in the in vitro preparation, and in vivo their concentration depends greatly on the state of vigilance of the brain.

We have performed manipulations to simulate some of the actions of neuromodulators with our model of a slowly oscillating cortical slice (see Figs. 15 and 14). We show that changing individual parameters of the model does not reproduce the most salient neurophysiological differences between

the slow-wave sleep and the waking states (Fig. 14). However, concomitant manipulations of adaptation currents, leakage K^+ currents, and recurrent excitation transformed a regularly oscillating network into a more irregular oscillating behavior (Fig. 15), closely resembling the slow oscillations observed during natural slow-wave sleep in unanesthetized cats (Steriade et al. 1996; Timofeev et al. 2001). Enhancement of the neuromodulator effects eventually brings the network into a tonic discharge state with no large-scale spatio-temporal coherence (but notice local coherent inhomogeneities in the multiunit record), reminiscent of typical cortical activity in the awake state (Destexhe et al. 1999; Steriade et al. 1996). This effect has been recently observed also in a thalamocortical network model of slow oscillations (Bazhenov et al. 2002). Unlike the in vivo observations, though, we find that in Fig. 15*B* the oscillations still propagate slowly across the network, whereas experiments have shown rapid synchronization of episodes across very long distances (Destexhe et al. 1999). A possibility is that the integrity of the corticothalamic feedback system has a synchronizing action on the cortically generated slow oscillation (Amzica and Steriade 1995; Contreras and Steriade 1997). However, the recently reported network model of Bazhenov et al. (2002) still shows slow wave propagation even in the presence of thalamocortical influences.

Our simulations were not meant to explore the myriad of known effects of neurotransmitters in the cerebral cortex. Specifically, the ability of acetylcholine and other neurotransmitters to enhance calcium-activated cation currents or to modulate activity differentially in subpopulations of cortical interneurons (Kawaguchi 1997, 1998) may be relevant in the natural transition from the sleep to waking and remain to be explored.

In summary, our model proposes that a given cortical microcircuit is more reverberatory during sleep than during waking states. Slow oscillations are a manifestation of both strong feedback synaptic excitation and neuronal adaptation during quiet sleep. A concomitant reduction by neuromodulators of recurrent excitatory synaptic transmission and adaptation currents leads to the transition to the tonic-firing state of wakefulness.

We thank C. Wilson and E. Stern for helpful discussions.

This work was supported by the National Institutes of Health (NIH), the Alfred P. Sloan Foundation, and the W. M. Keck Foundation to X.-J. Wang and A. Compte; by grants GV00-138-3 (Generalitat Valenciana) and PM98-0102-CO2-01 (Dirección General de Investigación, Spain) to M. V. Sanchez-Vives; and by the NIH to D. A. McCormick.

REFERENCES

Achermann P and Borbély AA. Low-frequency (<1 Hz) oscillations in the human sleep electroencephalogram. *Neuroscience* 81: 213–222, 1997.

Amzica F and Steriade M. Disconnection of intracortical synaptic linkages disrupts synchronization of a slow oscillation. *J Neurosci* 15: 4658–4677, 1995.

Bazhenov M, Timofeev I, Steriade M, and Sejnowski J. Model of thalamocortical slow-wave sleep oscillations and transitions to activated states. *J Neurosci* 22: 8691–8704, 2002.

Bischoff U, Vogel W, and Safronov BV. Na^+-activated K^+ channels in small dorsal root ganglion neurons of rat. *J Physiol* 510: 743–754, 1998.

Bressloff PC. Traveling waves and pulses in a one-dimensional network of excitable integrate-and-fire neurons. *J Math Biol* 40: 169–198, 2000.

Bullock TH and McClune MC. Lateral coherence of the electrocorticogram: a new measure of brain synchrony. *Electroencephalogr Clin Neurophysiol* 73: 479–498, 1989.

Buzás P, Eysel UT, Andorján P, and Kisvárday Z. Axonal topography of cortical basket cells in relation to orientation, direction, and ocular dominance maps. *J Comp Neurol* 437: 259–285, 2001.

Compte A, Brunel N, Goldman-Rakic PS, and Wang X-J. Synaptic mechanisms and network dynamics underlying spatial working memory in a cortical network model. *Cereb Cortex* 10: 910–923, 2000.

Constanti A and Sim JA. Calcium-dependent potassium conductance in guinea-pig olfactory cortex neurones in vitro. *J Physiol* 387: 173–194, 1987.

Contreras D and Steriade M. Synchronization of low-frequency rhythms in corticothalamic networks. *Neuroscience* 76: 11–24, 1997.

Contreras D, Timofeev I, and Steriade M. Mechanisms of long-lasting hyperpolarizations underlying slow sleep oscillations in cat corticothalamic networks. *J Physiol* 494: 251–264, 1996.

Cowan RL and Wilson CJ. Spontaneous firing patterns and axonal projections of single corticostriatal neurons in the rat medial agranular cortex. *J Neurophysiol* 71: 17–32, 1994.

Crook JM, Kisvárday ZF, and Eysel UT. Evidence for a contribution of lateral inhibition to orientation tuning and direction selectivity in cat visual cortex: reversible inactivation of functionally characterized sites combined with neuroanatomical tracing techniques. *Eur J Neurosci* 10: 2056–2075, 1998.

Destexhe A, Contreras D, and Steriade M. Spatiotemporal analysis of local field potentials and unit discharges in cat cerebral cortex during natural wake and sleep states. *J Neurosci* 19: 4595–4608, 1999.

Ermentrout B. The analysis of synaptically generated travelling waves. *J Comput Neurosci* 5: 191–208, 1998a.

Ermentrout GB. Neural networks as spatio-temporal pattern-forming systems. *Rep Prog Phys* 61: 353–430, 1998b.

Evarts EV. Temporal patterns of discharge of pyramidal tract neurons during sleep and waking in the monkey. *J Neurophysiol* 27: 152–171, 1964.

Fleidervish IA, Friedman A, and Gutnick MJ. Slow inactivation of Na^+ current and slow cumulative spike adaptation in mouse and guinea pig neocortical neurones in slices. *J Physiol* 493: 83–97, 1996.

Foehring RC, Schwindt PC, and Crill WE. Norepinephrine selectively reduces Ca^{2+}- and Na^+-mediated K^+ currents in cat neocortical neurons. *J Neurophysiol* 61: 245–256, 1989.

Fuhrmann G, Markram H, and Tsodyks M. Spike frequency adaptation and neocortical rhythms. *J Neurophysiol* 88: 761–770, 2002.

Gilbert CD and Wiesel TN. Clustered intrinsic connections in cat visual cortex. *J Neurosci* 3: 1116–1133, 1983.

Goldman MS, Golowasch J, Marder E, and Abbott LF. Global structure, robustness and modulation of neuronal models. *J Neurosci* 21: 5229–5238, 2001.

Golomb D and Amitai Y. Propagating neuronal discharges in neocortical slices: computational and experimental study. *J Neurophysiol* 78: 1199–1211, 1997.

Golomb D and Ermentrout GB. Bistability in pulse propagation in networks of excitatory and inhibitory populations. *Phys Rev Lett* 86: 4179–4182, 2001.

Golomb D and Ermentrout GB. Slow excitation supports propagation of slow pulses in networks of excitatory and inhibitory populations. *Phys Rev E* 65: 061911, 2002.

Gray CM, Konig P, Enkel AK, and Singer W. Oscillatory responses in cat visual cortex exhibit inter-columnar synchronization which reflects global stimulus properties. *Nature* 338: 334–337, 1989.

Hasselmo ME and Fehlau BP. Differences in time course of ACh and GABA modulation of excitatory synaptic potentials in slices of rat hippocampus. *J Neurophysiol* 86: 1792–1802, 2001.

Hubel D. Single-unit activity in striate cortex of unrestrained cats. *J Physiol* 147: 226–238, 1959.

Kawaguchi Y. Selective cholinergic modulation of cortical GABAergic cell subtypes. *J Neurophysiol* 78: 1743–1747, 1997.

Kawaguchi Y. Noradrenergic excitation and inhibition of GABAergic cell types in rat frontal cortex. *J Neurosci* 18: 6963–6976, 1998.

Kimura F and Baughman RW. Distinct muscarinic receptor subtypes suppress excitatory and inhibitory synaptic responses in cortical neurons. *J Neurophysiol* 77: 709–716, 1997.

Kimura F, Fukuda M, and Tsumoto T. Acetylcholine suppresses the spread of excitation in the visual cortex revealed by optical recording: possible differential effect depending on the source of input. *Eur J Neurosci* 11: 3597–3609, 1999.

Lampl I, Reichova I, and Ferster D. Synchronous membrane potential fluctuations in neurons of the cat visual cortex. *Neuron* 22: 361–374, 1999.

Li YX, Bertram R, and Rinzel J. Modeling *N*-methyl-D-aspartate-induced bursting in dopamine neurons. *Neuroscience* 71: 397–410, 1996.

Liu Y. *Dynamics of Cortical Neuronal Activity Across Multiple Temporal Scales: From Sensory Adaptation to Working Memory* (PhD thesis). Waltham, MA: Brandeis University.

Lund JS and Wu CQ. Local circuit neurons of macaque monkey striate cortex. IV. Neurons of laminae 1-3A. *J Comp Neurol* 384: 109–126, 1997.

Massimini M and Amzica F. Extracellular calcium fluctuations and intracellular potentials in the cortex during the slow sleep oscillation. *J Neurophysiol* 85: 1346–1350, 2001.

McCormick DA. Neurotransmitter actions in the thalamus and cerebral cortex and their role in neuromodulation of thalamocortical activity. *Prog Neurobiol* 39: 337–388, 1992.

Metherate R and Ashe JH. Ionic flux contributions to neocortical slow waves and nucleus basalis-mediated activation: whole cell recordings in vivo. *J Neurosci* 13: 5312–5323, 1993.

Nicoll RA, Malenka RC, and Kauer J. Functional comparison of neurotransmitter receptor subtypes in mammalian central nervous system. *Physiol Rev* 70: 513–565, 1990.

Nisenbaum ES, Xu ZC, and Wilson CJ. Contribution of a slowly inactivating potassium current to the transition to firing of neostriatal spiny projection neurons. *J Neurophysiol* 71: 1174–1189, 1994.

Osan R, Rubin J, and Ermentrout B. Regular traveling waves in a one-dimensional network of theta neurons. *SIAM J Appl Math* 62: 1197–1221, 2002.

Paré D, Shink E, Gaudreau H, Destexhe A, and Lang EJ. Impact of spontaneous synaptic activity on the resting properties of cat neocortical pyramidal neurons in vivo. *J Neurophysiol* 79: 1450–1460, 1998.

Pinsky PF and Rinzel J. Intrinsic and network rhythmogenesis in a reduced traub model for CA3 neurons. *J Comput Neurosci* 1: 39–60, 1994.

Rockland KS. Anatomical organization of primary visual cortex (area 17) in the ferret. *J Comp Neurol* 241: 225–236, 1985.

Sanchez-Vives MV and McCormick DA. Cellular and network mechanisms of rhythmic recurrent activity in neocortex. *Nat Neurosci* 3: 1027–1034, 2000.

Sanchez-Vives MV, Nowak LG, and McCormick DA. Cellular mechanisms of long-lasting adaptation in visual cortical neurons in vitro. *J Neurosci* 20: 4286–4299, 2000.

Schulz DW and Macdonald RL. Barbiturate enhancement of GABA-mediated inhibition and activation of chloride ion conductance: correlation with anticonvulsant and anesthetic actions. *Brain Res* 209: 177–188, 1981.

Schwindt PC, Spain WJ, and Crill WE. Long-lasting reduction of excitability by a sodium-dependent potassium current in cat neocortical neurons. *J Neurophysiol* 61: 233–244, 1989.

Seeger T and Alzheimer C. Muscarinic activation of inwardly rectifying K^+ conductance reduces EPSPs in rat hippocampal CA1 pyramidal cells. *J Physiol* 535: 383–396, 2001.

Spain WJ, Schwindt PC, and Crill WE. Anomalous rectification in neurons from cat sensorimotor cortex in vitro. *J Neurophysiol* 57: 1555–1576, 1987.

Steriade M, Amzica F, and Contreras D. Synchronization of fast (30-40 Hz) spontaneous cortical rhythms during brain activation. *J Neurosci* 16: 392–417, 1996.

Steriade M, Deschênes M, and Oakson G. Inhibitory processes and interneuronal apparatus in motor cortex during sleep and waking. I. Background firing and responsiveness of pyramidal tract neurons and interneurons. *J Neurophysiol* 37: 1065–1092, 1974.

Steriade M, Jones EG, and McCormick DA. *Thalamus: Organization and Function.* Oxford, UK: Elsevier, 1997.

Steriade M and McCarley RW. *Brain Stem Control of Wakefulness and Sleep.* New York: Plenum, 1990.

Steriade M, McCormick DA, and Sejnowski T. Thalamocortical oscillations in the sleeping and aroused brain. *Science* 262: 679–685, 1993a.

Steriade M, Núñez A, and Amzica F. A novel slow (<1 Hz) oscillation of neocortical neurons in vivo: depolarizing and hyperpolarizing components. *J Neurosci* 13: 3252–3265, 1993b.

Steriade M, Núñez A, and Amzica F. Intracellular analysis of relations between the slow (<1 Hz) neocortical oscillation and other sleep rhythms of the electroencephalogram. *J Neurosci* 13: 3266–3283, 1993c.

Steriade M, Timofeev I, and Grenier F. Natural waking and sleep states: a view from inside neocortical neurons. *J Neurophysiol* 85: 1969–1985, 2001.

Stern EA, Kincaid AE, and Wilson CJ. Spontaneous subthreshold membrane potential fluctuations and action potential variability of rat corticostriatal and striatal neurons in vivo. *J Neurophysiol* 77: 1697–1715, 1997.

Tabak J, Senn W, O'Donovan MJ, and Rinzel J. Modeling of spontaneous activity in developing spinal cord using activity-dependent depression in an excitatory network. *J Neurosci* 20: 3041–3056, 2000.

Timofeev I, Grenier F, Bazhenov M, Sejnowski TJ, and Steriade M. Origin of slow cortical oscillations in deafferented cortical slabs. *Cereb Cortex* 10: 1185–1199, 2000a.

Timofeev I, Grenier F, and Steriade M. Impact of intrinsic properties and synaptic factors on the activity of neocortical networks in vivo. *J Physiol* 94: 343–355, 2000b.

Timofeev I, Grenier F, and Steriade M. Disfacilitation and active inhibition in the neocortex during the natural sleep-wake cycle: an intracellular study. *Proc Natl Acad Sci USA* 98: 1924–1929, 2001.

Tsodyks M, Kenet T, Grinvald A, and Arieli A. Linking spontaneous activity of single cortical neurons and the underlying functional architecture. *Science* 286: 1943–1946, 1999.

Tsodyks MV and Markram H. The neural code between neocortical pyramidal neurons depends on neurotransmitter release probability. *Proc Natl Acad Sci USA* 94: 719–723, 1997.

Valentino RJ and Dingledine R. Presynaptic inhibitory effect of acetylcholine in the hippocampus. *J Neurosci* 1: 784–792, 1981.

van Vreeswijk C and Hansel D. Patters of synchrony in neural networks with spike adaptation. *Neural Comput* 13: 959–992, 2001.

Wang X-J. Calcium coding and adaptive temporal computation in cortical pyramidal neurons. *J Neurophysiol* 79: 1549–1566, 1998.

Wang X-J. Fast burst firing and short-term synaptic plasticity: a model of neocortical chattering neurons. *Neuroscience* 89: 347–362, 1999a.

Wang X-J. Synaptic basis of cortical persistent activity: the importance of NMDA receptors to working memory. *J Neurosci* 19: 9587–9603, 1999b.

Wang X-J. Synaptic reverberation underlying mnemonic persistent activity. *Trends Neurosci* 24: 455–463, 2001.

Wang X-J and Buzsáki G. Gamma oscillation by synaptic inhibition in a hippocampal interneuronal network model. *J Neurosci* 16: 6402–6413, 1996.

Wang X-J, Liu YH, Sanchez-Vives MV, and McCormick DA. Adaptation and temporal decorrelation by single neurons in the primary visual cortex. *J Neurophysiol* In press.

Wang Z and McCormick DA. Control of firing mode of corticotectal and corticopontine layer V burst generating neurons by norepinephrine, acetylcholine and 1S,3R-ACPD. *J Neurosci* 13: 2199–2216, 1992.

Wilson CJ. Dendritic morphology, inward rectification and the functional properties of neostriatal neurons. In: *Single Neuron Computation,* edited by McKenna T, Davis J, and Zornetzer SF. San Diego, CA: Academic, 1992, p. 141–171.

Wilson CJ and Kawaguchi Y. The origins of two-state spontaneous membrane potential fluctuations of neostriatal spiny neurons. *J Neurosci* 16: 2397–2410, 1996.

Wu J-y, Li G, Li B, and Yang Q. Spatiotemporal properties of an evoked population activity in rat sensory cortical slices. *J Neurophysiol* 86: 2461–2474, 2001.